

Neutrino and antineutrino charge-exchange reactions on ^{12}C

A. R. Samana^{1,2}, F. Krmpotić³, N. Paar⁴, and C. A. Bertulani¹

¹ *Department of Physics, Texas A&M University Commerce, P.O.3011 Commerce, 75429 TX, USA*

² *Departamento de Ciências Exactas e Tecnológicas, Universidade Estadual de Santa Cruz, CEP 45662-000 Ilhes, Bahia-BA, Brazil*

³ *Instituto de Física La Plata, CONICET, Facultad de Ciencias Astronómicas y Geofísicas, Universidad Nacional de La Plata, 1900 La Plata, Argentina, and*

⁴ *Physics department, Faculty of Science, University of Zagreb, Croatia*

(Dated: August 27, 2018)

We extend the formalism of weak interaction processes, obtaining new expressions for the transition rates, which greatly facilitate numerical calculations, both for neutrino-nucleus reactions and muon capture. Explicit violation of CVC hypothesis by the Coulomb field, as well as development of a sum rule approach for the inclusive cross sections have been worked out. We have done a thorough study of exclusive (ground state) properties of ^{12}B and ^{12}N within the projected quasi-particle random phase approximation (PQRPA). Good agreement with experimental data achieved in this way put in evidence the limitations of standard RPA and the QRPA models, which come from the inability of the RPA in opening the $p_{3/2}$ shell, and from the non-conservation of the number of particles in the QRPA. The inclusive neutrino/antineutrino ($\nu/\bar{\nu}$) reactions $^{12}\text{C}(\nu, e^-)^{12}\text{N}$ and $^{12}\text{C}(\bar{\nu}, e^+)^{12}\text{B}$ are calculated within both the PQRPA, and the relativistic QRPA (RQRPA). It is found that the magnitudes of the resulting cross-sections: i) are close to the sum-rule limit at low energy, but significantly smaller than this limit at high energies both for ν and $\bar{\nu}$, ii) they steadily increase when the size of the configuration space is augmented, and particularly for $\nu/\bar{\nu}$ energies > 200 MeV, and iii) converge for sufficiently large configuration space and final state spin. The quasi-elastic $^{12}\text{C}(\nu, \mu^-)^{12}\text{N}$ cross section recently measured in the MiniBooNE experiment is briefly discussed. We study the decomposition of the inclusive cross-section based on the degree of forbiddenness of different multipoles. A few words are dedicated to the $\nu/\bar{\nu}$ - ^{12}C charge-exchange reactions related with astrophysical applications.

PACS numbers: 23.40.-s, 25.30.Pt, 26.50.+x

I. INTRODUCTION

The massiveness of neutrinos and the related oscillations are strongly sustained by many experimental works involving atmospheric, solar, reactor and accelerator neutrinos [1–7]. The subsequent experimental goal is to determine precisely the various parameters of the Pontecorvo-Maki-Nakagawa-Sakata (PMNS) neutrino mass matrix, absolute masses of different flavors of neutrinos, CP violation in neutrino sector, etc. To address these problems several analyses of neutrino oscillation data are presently going on. At the same time, several experiments presently collect data, and others are planned. Accelerator experiments, experiments with neutrinos from ν -factories, β -beams, etc., are also planned and designed, as well as some experiments with natural ν -sources like solar neutrinos, atmospheric neutrinos, or antineutrinos from nuclear reactors.

The neutrino-nucleus scattering on ^{12}C is important because this nucleus is a component of many liquid scintillator detectors. Experiments such as LSND [1, 2], KARMEN [8, 9], and LAMPF [10, 11] have used ^{12}C to search for neutrino oscillations, and for measuring neutrino-nucleus cross sections. Present atmospheric and accelerator based neutrino oscillation experiments also involve ^{12}C , and operate at neutrino energies $E_\nu \sim 1$ GeV in order to access the relevant regions of oscillation parameter space. This is the case of the SciBar detec-

tor [12], where the molecule C_8H_8 is involved, and the MiniBooNE detector [13], which uses the light mineral oil containing the molecule CH_2 . The ^{12}C target will be used in several planned experiments, such as the spallation neutron source (SNS) at Oak Ridge National Laboratory (ORNL) [14], and the LVD (Large Volume Detector) experiment [15], developed by the INFN in Gran Sasso.

For the planned experimental searches of supernovae neutrino signals, which involve ^{12}C as scintillator liquid detector, the precise knowledge of neutrino cross sections of ^{12}N and ^{12}B ground-states, *i.e.*, of $\sigma_{e^-}(E_\nu, 1_1^+)$, and $\sigma_{e^+}(E_{\bar{\nu}}, 1_1^+)$ is very important. In fact, in the LVD experiment [15] the number of events detected during the supernova explosion are estimated by convoluting the neutrino supernova flux with: i) the interaction cross sections, ii) the efficiency of the detector, and iii) the number of target nuclei. For the carbon content of the LVD detector have been used so far $\sigma_{e^-}(E_\nu, 1_1^+)$, and $\sigma_{e^+}(E_{\bar{\nu}}, 1_1^+)$, as obtained from the Elementary Particle Treatment (EPT) [16]. Moreover, as an update of the LVD experiment related to supernovae neutrinos detection (where ^{12}C will also be employed), there is ongoing design study concerning large size scintillator detectors, called LAGUNA, where a 50 kt scintillator LENA is being considered [17].

On the other hand, as the ^{12}C nucleus forms one of the onion-like shells of a large star before collapse, it is also

important for astrophysics studies. Concomitantly, several authors [15, 18–23] have recently stressed the importance of measuring supernova neutrino oscillations. They claim that a supernova explosion represents a unique scenario for further study of the PMNS matrix. The corresponding neutrinos, which carry all flavors were observed in only one occasion (SN1987A), have an energy $E_\nu \lesssim 100$ MeV [24], and are also studied through the interactions with carbon nuclei in the liquid scintillator.

Thus, the main interest in the neutrino/antineutrino- ^{12}C charge-exchange cross sections comes from the neutrino oscillations, and precise knowledge of the cross sections in the neutrino energies going from a few MeVs up to a few GeVs is required. Up to quite recently the only available experimental information on reactions was that for the flux-averaged cross-sections: i) $^{12}\text{C}(\nu_e, e^-)^{12}\text{N}$ in the DAR region: $E_{\nu_e} < 60$ MeV [25–27], and ii) $^{12}\text{C}(\nu_\mu, \mu^-)^{12}\text{N}$ in the DIF region: $127 \text{ MeV} \leq E_{\nu_\mu} \leq 300$ MeV [28–30]. In last few years, however, several experimental programs at MiniBooNE [31], K2K [32], and SciBooNE [33] yield results on the $(\nu_\mu, ^{12}\text{C})$ cross section for $0.4 \text{ GeV} \leq E_{\nu_\mu} \leq 1.7 \text{ GeV}$. It is well known that for E_ν larger than a few hundreds MeV's, besides the quasi-elastic (QE) channel, many inelastic channels are open and pion production becomes important. In fact, there have been quite active experimental efforts to investigate neutrino-induced coherent single-pion production in the Δ -excitation region of ^{12}C . Starting approximately at the threshold coming from the pion and charged lepton masses (m_π and m_ℓ), the $\pi + \ell$ production cross section steadily increases with the neutrino energy becoming larger than the quasi-elastic one for $E_\nu \lesssim 1.5 \text{ GeV}$ [31–33].

From the theoretical side there have been great efforts to understand the nuclear structure within the triad $\{^{12}\text{B}, ^{12}\text{C}, ^{12}\text{N}\}$. In the seminal work of O'Connell, Donnelly, and Walecka [34] a unified analysis of electromagnetic, and semileptonic weak interactions was presented. To describe the nuclear dynamics they have used the particle-hole Tamm-Dancof Approximation (TDA) within a very small single-particle space $^1 (S_2 \equiv \{1s_{1/2}, 1p_{3/2}, 1p_{1/2}, 1d_{5/2}, 2s_{1/2}\})$ [35]. To achieve agreement with experiments for the β^\pm -decays, and μ -capture they were forced to use an overall reduction factor ξ^2 of the order of 4 (2) for even (odd) parity states. They have also pointed out that this factor would become totally unnecessary with use of a better nuclear model able to open the $1p_{3/2}$ shell.

Rather thorough comparisons of $2s1d$ and $2p1f$ shell-model predictions with measured allowed β -decay rates have yielded a simple, phenomenological effective axial coupling $g_A = 1$ that should be used rather than the bare value [36–39]. This observation is the basis for many

nuclear model estimates of the Gamow-Teller (GT) response that governs allowed neutrino cross sections. In Ref. [34] $g_A = 1.23$ was used based on a study of neutron β -decay, and, as the analyzed processes were dominantly of the axial-vector type, the use of $g_A = 1$ would have diminished the reduction factors ξ^2 in an appreciable way.

In the Random Phase Approximation (RPA), besides the TDA forward-going amplitudes, the backward-going amplitudes are present as well. However, these additional RPA amplitudes did not help to open the $1p_{3/2}$ shell in the continuum RPA (CRPA) calculations of Kolbe, Langanke, and Krewald [40]. Thus, as in the case of the TDA used in Ref. [34], to get agreement with data for the ground state triplet $T = 1$ (β^\pm -decays, μ -capture, and the exclusive $^{12}\text{C}(\nu_e, e^-)^{12}\text{N}$ reaction) their calculations were rescaled by a factor $\cong 4$.

The main aim of the CRPA is to describe appropriately not only the bound states but also the virtual (quasi-bound), resonant, and continuum states, which are treated as bound states in the RPA. However, this superiority has not been evidenced so far in numerical calculations. For instance, in the case of μ -capture rates in ^{16}N the two methods agree with each other quite well for the 0^- and 1^- states, while the RPA result is preferred for the 2^- state [41].

To open the $1p_{3/2}$ shell one has to introduce pairing correlations. This is done within the Shell Model (SM) [42–44], which reproduces quite well both i) the experimental flux-averaged exclusive, and inclusive cross sections for the $^{12}\text{C}(\nu_e, e^-)^{12}\text{N}$ DAR [25–27], and $^{12}\text{C}(\nu_\mu, \mu^-)^{12}\text{N}$ DIF [28] reactions, and ii) the $\mu^- + ^{12}\text{C} \rightarrow \nu_\mu + ^{12}\text{B}$ muon-capture modes [45–47].

The quasiparticle RPA (QRPA) also opens the $1p_{3/2}$ shell by means of the pairing interaction. However, it fails as well in accounting for the exclusive processes to the isospin triplet $T = 1$ in ^{12}C , because a new problem emerges, as first observed by Volpe *et al.* [43]. They noted that within the QRPA the lowest state in ^{12}N irremediably turned out not to be the most collective one. Later it was shown [48–50] that: 1) the origin of this difficulty arises from the degeneracy among the four lowest proton-neutron two-quasiparticle ($2qp$) states $|1p_{1/2}1p_{3/2}\rangle$, $|1p_{3/2}1p_{3/2}\rangle$, $|1p_{1/2}1p_{1/2}\rangle$ and $|1p_{3/2}1p_{1/2}\rangle$, which, in turn, comes from the fact that for $N = Z = 6$ the quasiparticle energies $E_{1p_{1/2}}$ and $E_{1p_{3/2}}$ are very close to each other, and 2) it is imperative to use the projected QRPA (PQRPA) for a physically sound description of the weak processes among the ground states of the triad $\{^{12}\text{B}, ^{12}\text{C}, ^{12}\text{N}\}$ [48–50]; see Figs. 2 and 3 in Ref. [49].

In summary, neither the CRPA nor the QRPA are the appropriate nuclear models to describe the “fine structure” of exclusive charge-exchange processes around ^{12}C , and they only can be used for global inclusive descriptions. Of course, the same is valid for the relativistic RPA (RQRPA) that has recently been applied with success in calculations of inclusive charged-current neutrino-nucleus reactions in ^{12}C , ^{16}O , ^{56}Fe , and ^{208}Pb [51], and total muon capture rates on a large set of nuclei from ^{12}C

¹ From now on a single-particle (s.p.) space that includes all orbitals within N harmonic oscillator (HO) shells will be labeled as space S_N .

to ^{244}Pu [52]. The continuum QRPA (CQRPA) would have to be superior to the QRPA for the same reasons that the CRPA would have to be better than the RPA. Nevertheless, neither this superiority has been put in evidence by numerical calculations [53, 54]. Finally, it is clear that the nuclear structure descriptions inspired on the Relativistic Fermi Gas Model (RFGM) [55–57], which do not involve multipole expansions, should only be used for inclusive quantities.

When the effects due to resonant and continuum states are considered, as it is done within the CRPA and CQRPA, the spreading in strength of the hole states in the inner shells should also be taken into account for the sake of consistency. In fact, a single-particle state j that is deeply bound in the parent nucleus, after a weak interacting process can become a highly excited hole-state j^{-1} in the continuum of the residual nucleus. There it is suddenly mixed with more complicated configurations (2h1p, 3h2p, . . . excitations, collective states, and so on) spreading its strength in a relatively wide energy interval [58]². This happens, for instance, with the $1s_{1/2}$ orbital in ^{12}C , that is separated from the $1p_{3/2}$ state by approximately 23 MeV, which is enough to break the 12 particle system, where the energy of the last excited state amounts to 11.5 MeV in ^{12}N , and 16.5 MeV in ^{12}B channels. Although the detailed structure and fragmentation of hole states are still not well known, the exclusive knockout reactions provide a wealth of information on the structure of single-nucleon states of nuclei. Excitation energies and widths of proton-hole states were systematically measured with quasifree (p, 2p) and ($e, e'p$) reactions, which revealed the existence of inner orbital shells in nuclei [59–67].

In the TDA calculation of Ref. [34] the S_2 space has been used, which extends only from 13.77 MeV up to 30.05 MeV, embracing, respectively, 1, 2, 2, 1, and 1 negative parity states $J^\pi = 0^-, 1^-, 2^-, 3^-$, and 4^- , and 1, 2, 2, and 1 positive parity states $J^\pi = 0^+, 1^+, 2^+$, and 3^+ . With such small configuration space, the neutrino cross sections $\sigma_e(E_\nu)$, and $\sigma_\mu(E_\nu)$ have been evaluated up to a neutrino energy E_ν of 0.6 GeV, and extrapolated up to 20 GeV. In recent years, however, large configuration spaces have been used in the evaluation of QE cross sections for $E_\nu \sim 1$ GeV. For instance, Amaro *et al.* [68] have employed the single-particle SM (TDA without the residual interaction) in a semirelativistic description of quasielastic neutrino reactions (ν_μ, μ^-) on ^{12}C going up to $E_\nu = 1.5$ GeV, and including multipoles $J^\pi \leq 47^\pm$. Good agreement with the RFGM was obtained for several choices of kinematics of interest for the ongoing neutrino oscillation experiments. Kolbe *et al.* [69] have also achieved an excellent agreement between the RFGM and the CRPA calculations of the total cross

section and the angular distribution of the outgoing electrons in $^{16}\text{O}(\nu_e, e)X$ for $E_\nu \leq 0.5$ GeV. They have considered states up to $J^\pi = 9^\pm$ only, and didn't specify the configuration space used. Moreover, Valverde *et al.* [57] have analyzed the theoretical uncertainties of the RFGM developed in [56] for the (ν_e, e^-), and (ν_μ, μ^-) cross sections in ^{12}C , ^{16}O , and ^{40}Ca for $E_\nu \leq 0.5$ GeV. The work of Kim *et al.* [70] should also be mentioned where were studied the effects of strangeness on the (ν_μ, μ^-) and ($\bar{\nu}_\mu, \mu^+$) cross sections in ^{12}C for incident energies between 0.5 MeV and 1.0 GeV, within the framework of a relativistic single-particle model. Quite recently, Butkevich [71] has also studied the scattering of muon neutrino on carbon targets for neutrino energies up to 2.8 GeV within a relativistic shell-model approach without specifying the model space.

For relatively large neutrino energies ($E_{\nu_e} \gtrsim m_\pi$, and $E_{\nu_\mu} \gtrsim m_\pi + m_\mu$) to the above-mentioned QE cross sections should be added the pion production cross section, as done, for instance, in Refs. [72, 73]. One should also note that $\sigma_e(E_{\nu_e})$ and $\sigma_\mu(E_{\nu_\mu})$ coincide with each other asymptotically. This is clearly put in evidence in the Extreme Relativistic Limit (ERL) where $|\mathbf{p}_\ell|/E_\ell \rightarrow 1$, and the neutrino-nucleus cross sections depend on m_ℓ only through the threshold energy, as can be seen from the Appendix C of the present work. The Figure 4 from Ref. [74] is also illustrative in this respect.

Therefore, we focus our attention only on the quasi-elastic cross section $\sigma_e(E_{\nu_e})$ since, at muon-neutrino energies involved in the MiniBooNE experiment [13], it is equal to $\sigma_\mu(E_{\nu_\mu})$ for all practical purposes.

One of main objectives in the present study is to analyze the effect of the size of the configuration space up to neutrino energies of several hundred MeV. As in several previous works [34, 39–44, 48–52, 57, 68–70, 74] this will be done in first order perturbation theory. The consequences of the particle-particle force in the S = 1, T = 0 channel, within the PQRPA will also be examined. The importance of this piece of the residual interaction was discovered more than 20 years ago by Vogel and Zirnbauer [75] and Cha [76], and since then the QRPA became the most frequently used nuclear structure method for evaluating double β -decay rates.

A few words will be devoted as well as to the non-relativistic formalisms for neutrino-nucleus scattering. The most popular one was developed by the Walecka group [34, 77–79], where the nuclear transition matrix elements are classified as Coulomb, longitudinal, transverse electric, and transverse magnetic multipole moments. We feel that these denominations might be convenient when discussing simultaneously charge-conserving, and charge-exchange processes, but seems unnatural when one considers only the last ones. As a matter of fact, this terminology is not often used in nuclear β -decay, μ -capture, and charge-exchange reactions where one only speaks of vector and axial matrix elements with different degrees of forbiddenness: allowed (GT and Fermi), first forbidden, second forbidden, *etc.*, types [80, 81]. There are excep-

² One should keep in mind that the mean life of ^{12}N and ^{12}B are, respectively, 11.0 and 20.2 ms, while strong interaction times are of the order of 10^{-21} s.

tions, of course, as for instance, is the recent work of Marketin *et al.* [52] on muon capture, where the Walecka's classification was used.

The formalism worked out by Kuramoto [74] is also frequently used for the evaluation of neutrino-nucleus cross-sections. It is simpler than that of Walecka, but it does not contain relativistic matrix elements, nor is applicable for muon capture rates.

More recently, we have introduced another formalism [48–50]. Besides of being almost as simple as that of Kuramoto, it retains relativistic terms and can be used for μ -capture. This formalism is briefly sketched here, including the consequences of the violation of the Conserved Vector Current (CVC) by the Coulomb field. It is furthermore simplified by classifying the nuclear matrix elements in natural and unnatural parities. We also show how within the present formalism both the sum rule approach, and the formula for ERL look like.

In Section II we briefly describe the formalism used to evaluate different weak interacting processes. Some details are delegated to the Appendices: A) Contributions of natural and unnatural parity states to the transition rates, B) Sum rule approach for the inclusive neutrino-nucleus cross section, C) Formula for the inclusive neutrino-nucleus cross section at the extreme relativistic limit, and D) Formula for the muon capture rate. In Section III we present, and discuss the numerical results. Comparisons with experimental data, as well as with previous theoretical studies, are done whenever possible. Here we firstly sketch the two theoretical frameworks, namely the PQRPA and RQRPA, used in the numerical calculations. In subsections II, and IIIB we present the results for the exclusive and inclusive processes, respectively. Finally, in Section IV we give a brief summary, and final conclusions.

II. FORMALISM FOR THE WEAK INTERACTING PROCESSES

The weak Hamiltonian is expressed in the form [77, 78, 82]

$$H_w(\mathbf{r}) = \frac{G}{\sqrt{2}} J_\alpha l_\alpha e^{-i\mathbf{r}\cdot\mathbf{k}}, \quad (2.1)$$

where $G = (3.04545 \pm 0.00006) \times 10^{-12}$ is the Fermi coupling constant (in natural units), the leptonic current $l_\alpha \equiv \{\mathbf{1}, i\mathbf{l}_\theta\}$ is given by the Eq. (2.3) in Ref. [49] and the hadronic current operator $J_\alpha \equiv \{\mathbf{J}, iJ_\theta\}$ in its non-

relativistic form reads³

$$\begin{aligned} J_\theta &= g_V + (\bar{g}_A + \bar{g}_{P1}) \boldsymbol{\sigma} \cdot \hat{\mathbf{k}} + g_A \frac{i\boldsymbol{\sigma} \cdot \nabla}{M}, \\ \mathbf{J} &= -g_A \boldsymbol{\sigma} - i\bar{g}_W \boldsymbol{\sigma} \times \hat{\mathbf{k}} - \bar{g}_V \hat{\mathbf{k}} + \bar{g}_{P2} (\boldsymbol{\sigma} \cdot \hat{\mathbf{k}}) \hat{\mathbf{k}} - g_V \frac{i\nabla}{M}, \end{aligned} \quad (2.2)$$

where $\hat{\mathbf{k}} \equiv \mathbf{k}/|\mathbf{k}|$. The quantity

$$k = P_i - P_f \equiv \{\mathbf{k}, ik_\theta\} \quad (2.3)$$

is the momentum transfer, M is the nucleon mass, and P_i and P_f are momenta of the initial and final nucleon (nucleus). The effective vector, axial-vector, weak-magnetism and pseudoscalar dimensionless coupling constants are, respectively

$$\begin{aligned} g_V &= 1, \quad g_A = 1, \quad g_M = \kappa_p - \kappa_n = 3.70, \\ g_P &= g_A \frac{2Mm_\ell}{k^2 + m_\pi^2}, \end{aligned} \quad (2.4)$$

where the following short notation has been introduced:

$$\begin{aligned} \bar{g}_V &= g_V \frac{\kappa}{2M}; \quad \bar{g}_A = g_A \frac{\kappa}{2M}; \quad \bar{g}_W = (g_V + g_M) \frac{\kappa}{2M}, \\ \bar{g}_{P1} &= g_P \frac{\kappa}{2M} \frac{k_\theta}{m_\ell}; \quad \bar{g}_{P2} = g_P \frac{\kappa}{2M} \frac{\kappa}{m_\ell}, \end{aligned} \quad (2.5)$$

where $\kappa \equiv |\mathbf{k}|$. The above estimates for g_M and g_P come from the conserved vector current (CVC) hypothesis, and from the partially conserved axial vector current (PCAC) hypothesis, respectively. The finite nuclear size (FNS) effect is incorporated via the dipole form factor with a cutoff $\Lambda = 850$ MeV, i.e., $g \rightarrow g [\Lambda^2/(\Lambda^2 + k^2)]^2$.

In performing the multipole expansion of the nuclear operators

$$O_\alpha \equiv (\mathbf{O}, iO_\theta) = J_\alpha e^{-i\mathbf{k}\cdot\mathbf{r}}, \quad (2.6)$$

it is convenient 1) to take the momentum \mathbf{k} along the z axis, i.e.,

$$\begin{aligned} e^{-i\mathbf{k}\cdot\mathbf{r}} &= \sum_{\mathbf{L}} i^{-L} \sqrt{4\pi(2L+1)} j_L(\rho) Y_{L0}(\hat{\mathbf{r}}), \\ &= \sum_{\mathbf{J}} i^{-J} \sqrt{4\pi(2J+1)} j_J(\rho) Y_{J0}(\hat{\mathbf{r}}), \end{aligned} \quad (2.7)$$

where $\rho = \kappa r$, and 2) to define the operators O_α as

$$O_\alpha = \sqrt{4\pi} \sum_{\mathbf{J}} i^{-J} \sqrt{2J+1} O_{\alpha\mathbf{J}}. \quad (2.8)$$

³ As in Ref. [49] we use the Walecka's notation [78] with the Euclidean metric for the quadrivectors, and $\alpha = 1, 2, 3, 4$. The only difference is that we substitute his indices (0, 3) by our indices ($\theta, 0$), where we use the index θ for the temporal component and the index 0 for the third spherical component.

In this way we avoid the troublesome factor i^{-J} . In spherical coordinates ($m = -1, 0, +1$) we have

$$\begin{aligned} J_0 &= g_V + (\bar{g}_A + \bar{g}_{P1})\sigma_0 + ig_A M^{-1} \boldsymbol{\sigma} \cdot \boldsymbol{\nabla} \\ J_m &= -g_A \sigma_m + m \bar{g}_W \sigma_m + \delta_{m0} [-\bar{g}_V + \bar{g}_{P2} \sigma_0] \\ &\quad - ig_V M^{-1} \nabla_m, \end{aligned} \quad (2.9)$$

and

$$\begin{aligned} O_{0J} &= j_J(\rho) Y_{J0}(\hat{\mathbf{r}}) J_0, \\ O_{mJ} &= \sum_L i^{J-L} F_{LJm} j_L(\rho) [Y_L(\hat{\mathbf{r}}) \otimes \mathbf{J}]_J, \end{aligned} \quad (2.10)$$

where

$$\begin{aligned} F_{LJm} &\equiv (-)^{J+m} \sqrt{2L+1} \begin{pmatrix} L & 1 & J \\ 0 & -m & m \end{pmatrix} \\ &= (-)^{1+m} (1, -m, J, m | L, 0), \end{aligned} \quad (2.11)$$

is a Clebsch-Gordan coefficient.⁴

Explicitly, from (2.9)

$$\begin{aligned} O_{0J} &= g_V \mathcal{M}_J^V + ig_A \mathcal{M}_J^A + i(\bar{g}_A + \bar{g}_{P1}) \mathcal{M}_{0J}^A, \\ O_{mJ} &= i(\delta_{m0} \bar{g}_{P2} - g_A + m \bar{g}_W) \mathcal{M}_{mJ}^A \\ &\quad + g_V \mathcal{M}_{mJ}^V - \delta_{m0} \bar{g}_V \mathcal{M}_J^V. \end{aligned} \quad (2.13)$$

The elementary operators are given by

$$\begin{aligned} \mathcal{M}_J^V &= j_J(\rho) Y_J(\hat{\mathbf{r}}), \\ \mathcal{M}_J^A &= M^{-1} j_J(\rho) Y_J(\hat{\mathbf{r}}) (\boldsymbol{\sigma} \cdot \boldsymbol{\nabla}), \end{aligned} \quad (2.14)$$

and

$$\begin{aligned} \mathcal{M}_{mJ}^A &= \sum_{L \geq 0} i^{J-L-1} F_{LJm} j_L(\rho) [Y_L(\hat{\mathbf{r}}) \otimes \boldsymbol{\sigma}]_J, \\ \mathcal{M}_{mJ}^V &= M^{-1} \sum_{L \geq 0} i^{J-L-1} F_{LJm} j_L(\rho) [Y_L(\hat{\mathbf{r}}) \otimes \boldsymbol{\nabla}]_J. \end{aligned} \quad (2.15)$$

The CVC relates the vector-current pieces of the operator (2.6) as (see Eqs. (10.45) and (9.7) from Ref. [81])

$$\mathbf{k} \cdot \mathbf{O}^V \equiv \kappa O_0^V = \tilde{k}_0 O_0^V, \quad (2.16)$$

with

$$\tilde{k}_0 \equiv k_0 - S(\Delta E_{\text{Coul}} - \Delta M), \quad (2.17)$$

⁴ Their values are:

$$\begin{aligned} F_{J+1, J, 0} &= -\sqrt{\frac{J+1}{2J+1}}, & F_{J-1, J, 0} &= \sqrt{\frac{J}{2J+1}}, \\ F_{J+1, J, \pm 1} &= \sqrt{\frac{J}{2(2J+1)}}, & F_{J, J-1, \pm 1} &= \sqrt{\frac{J+1}{2(2J+1)}}, \\ F_{J, J, 0} &= 0, & F_{J, J, \pm 1} &= \mp \frac{1}{\sqrt{2}}. \end{aligned}$$

where

$$\Delta E_{\text{Coul}} \cong \frac{6e^2 Z}{5R} \cong 1.45 Z A^{-1/3} \text{ MeV}, \quad (2.18)$$

is the Coulomb energy difference between the initial and final nuclei, $\Delta M = M_n - M_p = 1.29$ MeV is the neutron-proton mass difference, and $S = \pm 1$ for neutrino and antineutrino scattering, respectively.

The consequence of the CVC relation (2.16) is the substitution

$$g_V \mathcal{M}_{0J}^V - \bar{g}_V \mathcal{M}_J^V \rightarrow \frac{\tilde{k}_0}{\kappa} g_V \mathcal{M}_J^V, \quad (2.19)$$

in (2.13), and O_{mJ} now reads

$$\begin{aligned} O_{mJ} &= i(\delta_{m0} \bar{g}_{P2} - g_A + m \bar{g}_W) \mathcal{M}_{mJ}^A \\ &\quad + |m| g_V \mathcal{M}_{mJ}^V + \delta_{m0} \frac{\tilde{k}_0}{\kappa} g_V \mathcal{M}_J^V. \end{aligned} \quad (2.20)$$

The second term in (2.17) comes from the violation of the CVC by the electromagnetic interaction. Although it is frequently employed in the nuclear β -decay, as far as we know, it has never been considered before in the neutrino-nucleus scattering. ΔE_{Coul} is equal to 3.8, 9.8, and 20.0 MeV for ^{12}C , ^{56}Fe , and ^{208}Pb , respectively, and therefore the just mentioned term could be quite significant, specially for heavy nuclei.

The transition amplitude for the neutrino-nucleus reaction at a fixed value of κ , from the initial state $|0^+\rangle$ in the (Z, N) nucleus to the n -th final state $|J_n^\pi\rangle$ in the nucleus $(Z \pm 1, N \mp 1)$, reads

$$\mathcal{T}_{J_n^\pi}(\kappa) \equiv \sum_{s_\ell, s_\nu} |\langle J_n^\pi | H_W(\kappa) | 0^+ \rangle|^2. \quad (2.21)$$

The momentum transfer here is $k = p_\ell - q_\nu$, with $p_\ell \equiv \{\mathbf{p}_\ell, iE_\ell\}$ and $q_\nu \equiv \{\mathbf{q}_\nu, iE_\nu\}$, and after some algebra [49] one gets

$$\begin{aligned} \mathcal{T}_{J_n^\pi}(\kappa) &= 4\pi G^2 \left[\sum_{\alpha=\theta, 0, \pm 1} |\langle J_n^\pi | O_{\alpha J}(\kappa) | 0^+ \rangle|^2 \mathcal{L}_\alpha \right. \\ &\quad \left. - 2\Re(\langle J_n^\pi | O_{0J}(\kappa) | 0^+ \rangle \langle J_n^\pi | O_{0J}(\kappa) | 0^+ \rangle^*) \mathcal{L}_{\theta 0} \right], \end{aligned} \quad (2.22)$$

where

$$\begin{aligned} \mathcal{L}_\theta &= 1 + \frac{|\mathbf{p}_\ell| \cos \theta}{E_\ell}, \\ \mathcal{L}_0 &= 1 + \frac{2q_0 p_0}{E_\ell E_\nu} - \frac{|\mathbf{p}_\ell| \cos \theta}{E_\ell}, \\ \mathcal{L}_{\pm 1} &= 1 - \frac{q_0 p_0}{E_\ell E_\nu} \pm \left(\frac{q_0}{E_\nu} - \frac{p_0}{E_\ell} \right) S, \\ \mathcal{L}_{\theta 0} &= \frac{q_0}{E_\nu} + \frac{p_0}{E_\ell}, \end{aligned} \quad (2.23)$$

are the lepton traces, with $\theta \equiv \hat{\mathbf{q}}_\nu \cdot \hat{\mathbf{p}}_\ell$ being the angle between the incident neutrino and ejected lepton momenta, and

$$\begin{aligned} q_0 &= \hat{k} \cdot \mathbf{q}_\nu = \frac{E_\nu (|\mathbf{p}_\ell| \cos \theta - E_\nu)}{\kappa}, \\ p_0 &= \hat{k} \cdot \mathbf{p}_\ell = \frac{|\mathbf{p}_\ell| (|\mathbf{p}_\ell| - E_\nu \cos \theta)}{\kappa}, \end{aligned} \quad (2.24)$$

the z -components of the neutrino and lepton momenta.

The exclusive cross-section (ECS) for the state $|J_n^\pi\rangle$, as a function of the incident neutrino energy E_ν , is

$$\sigma_\ell(J_n^\pi, E_\nu) = \frac{|\mathbf{p}_\ell| E_\ell}{2\pi} F(Z + S, E_\ell) \int_{-1}^1 d(\cos\theta) \mathcal{T}_{J_n^\pi}(\kappa), \quad (2.25)$$

where

$$\begin{aligned} E_\ell &= E_\nu - \omega_{J_n^\pi}, \quad |\mathbf{p}_\ell| = \sqrt{(E_\nu - \omega_{J_n^\pi})^2 - m_\ell^2}, \\ \kappa &= |\mathbf{p}_\ell - \mathbf{q}_\nu| \\ &= \sqrt{2E_\nu(E_\ell - |\mathbf{p}_\ell| \cos\theta) - m_\ell^2 + \omega_{J_n^\pi}^2}, \end{aligned} \quad (2.26)$$

and $\omega_{J_n^\pi} = -k_0 = E_\nu - E_\ell$ is the excitation energy of the state $|J_n^\pi\rangle$ relative to the state $|0^+\rangle$. Moreover, $F(Z + S, E_\ell)$ is the Fermi function for neutrino ($S = 1$), and antineutrino ($S = -1$), respectively.

As it well known the charged-current cross sections must be corrected for the distortion of the outgoing lepton wave function by the Coulomb field of the daughter nucleus. For relatively low neutrino energies ($\sim 40 - 50$ MeV) this correction was implemented by numerical solution of the Dirac equation for an extended nuclear charge [81]. At higher energies, the effect of the Coulomb field was described by the effective momentum approximation (EMA) [83], in which the lepton momentum p_ℓ and energy E_ℓ are modified by the corresponding effective quantities (see [51, Eq. (34) and (45)]).

Here, we will also deal with inclusive cross-section (ICS),

$$\sigma_\ell(E_\nu) = \sum_{J_n^\pi} \sigma_\ell(J_n^\pi, E_\nu), \quad (2.27)$$

as well as with folded cross-sections, both exclusive,

$$\bar{\sigma}_\ell(J_n^\pi) = \int dE_\nu \sigma_\ell(J_n^\pi, E_\nu) n_\ell(E_\nu), \quad (2.28)$$

and inclusive

$$\bar{\sigma}_\ell = \int dE_\nu \sigma_\ell(E_\nu) n_\ell(E_\nu), \quad (2.29)$$

where $n_\ell(E_\nu)$ is the neutrino (antineutrino) normalized flux. In the evaluation of both neutrino, and antineutrino ICS the summation in (2.27) goes over all n states with spin and parity $J^\pi \leq 7^\pm$ in the PQRPA, and over $J^\pi \leq 14^\pm$ in the RQRPA.

In the Appendix A we show that the real and imaginary parts of the operators $\mathcal{O}_{\alpha J}$, given by (2.12) and (2.20), contribute to natural and unnatural parity states, respectively. This greatly simplifies the numerical calculations, because one always deals with real operators only. In Appendix D are also shown the formula for the muon capture process within the present formalism.

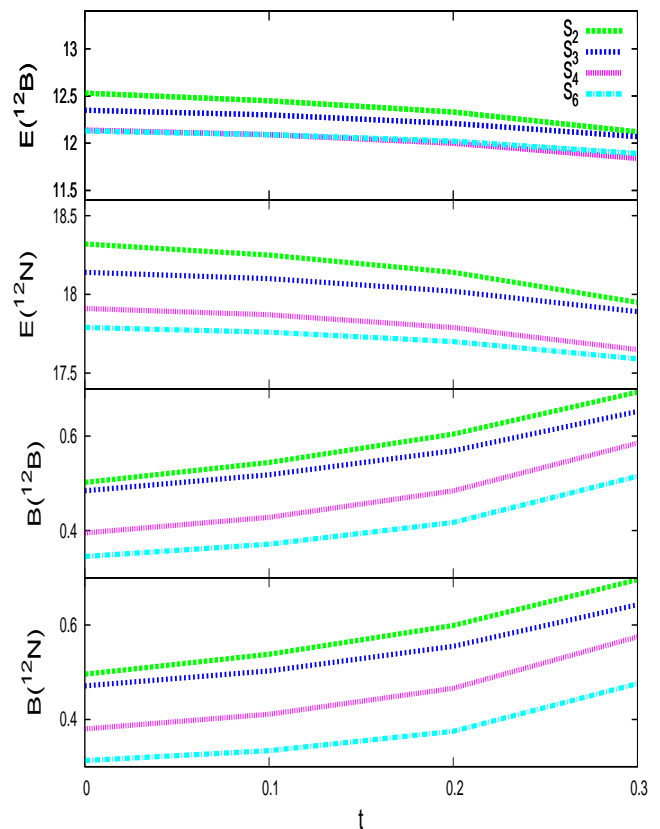


FIG. 1: (Color online) ^{12}B and ^{12}N ground state energies (in units of MeV) and GT B -values within the PQRPA for different s.p. spaces, as function of the pp -coupling t . The experimental values are: $E(^{12}\text{B}) = 13.37$ MeV, and $E(^{12}\text{N}) = 17.33$ MeV [95], and $B(^{12}\text{B}) = 0.466$, and $B(^{12}\text{N}) = 0.526$ [96].

III. NUMERICAL RESULTS AND DISCUSSION

The major part of the numerical calculations have been done within the PQRPA by employing the δ -interaction (in MeV fm^3)

$$V = -4\pi (v_s P_s + v_t P_t) \delta(r),$$

with singlet (v_s), and triplet (v_t) coupling constants different for the particle-hole (ph), particle-particle (pp), and pairing ($pair$) channels [84]. This interaction leads to a good description of single and double β -decays and it has been used extensively in the literature [85–88]. The single-particle wave functions were approximated with those of the HO with the length parameter $b = 1.67$ fm, which corresponds to the oscillator energy $\hbar\omega = 45A^{-1/3} - 25A^{-2/3}$ MeV. The s.p. spaces S_2, S_3, S_4 , and S_6 will be explored.

In Refs. [48, 49], where the S_3 space was used, we have pointed out that the values of the coupling strengths v_s^{pp} , v_s^{pair} , and v_t^p used in $N > Z$ nuclei ($v_s^{pp} = v_s^{pair}$, $v_t^p \gtrsim v_s^{pp}$), might not be suitable for $N = Z$ nuclei. In fact, the best agreement with data in ^{12}C is obtained for: i) the energy of the ground state in ^{12}N , $E(^{12}\text{N})$, ii) the GT B -values in ^{12}C , $B(^{12}\text{N})$ and $B(^{12}\text{B})$, and iii) the exclusive

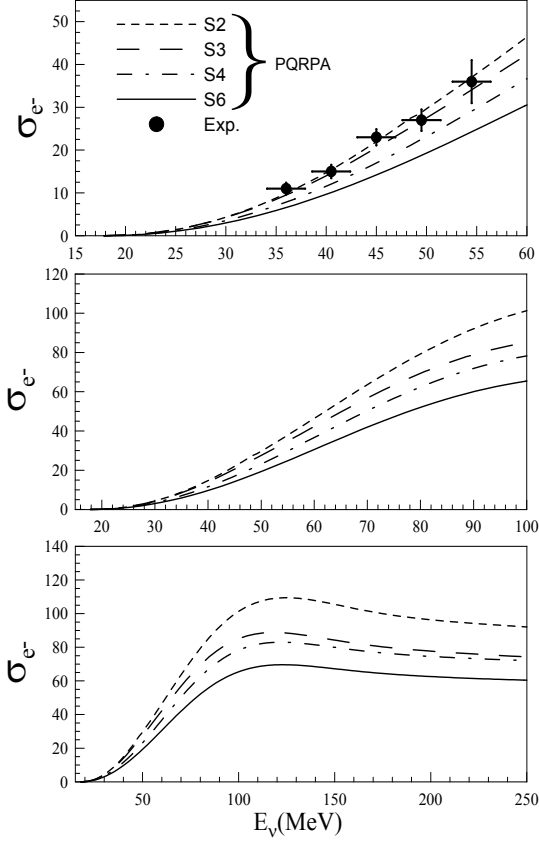


FIG. 2: Exclusive $^{12}\text{C}(\nu, e^-)^{12}\text{N}$ cross-section $\sigma_{e^-}(E_\nu, 1_1^+)$ (in units of 10^{-42} cm^2), plotted as a function of the incident neutrino energy E_ν . Results for several single-particle spaces S_N , and $t = 0$, within three different energy intervals, are shown. The experimental data in the DAR region are from Ref. [25].

muon capture in ^{12}B , $\Lambda^{\text{exc}} \equiv \Lambda(1_1^+)$, is obtained when the pp channel is totally switched off, i.e., $v_s^{pp} \equiv v_t^{pp} = 0$. The adopted ph coupling strengths are $v_s^{ph} = 27 \text{ MeV fm}^3$ and $v_t^{ph} = 64 \text{ MeV fm}^3$ [48]. For the pp channel it is convenient to define the parameters

$$s = \frac{v_s^{pp}}{v_s^{pair}}, \quad t = \frac{v_t^{pp}}{v_s^{pair}},$$

where $v_s^{pair} = (v_s^{pair}(p) + v_s^{pair}(n))/2$ [88]. As in our previous work on ^{12}C , we will use here the same singlet and triplet pp couplings, i.e., $s \equiv t$ [48, 49]. The states with $J^\pi = 0^+$, and $J^\pi = 1^+$ only depend on s , and t , respectively, while all remaining depend on both coupling strengths.

The s.p. energies and pairing strengths for S_2 , S_3 , and S_4 spaces, were varied in a χ^2 search to account for the experimental spectra of odd-mass nuclei ^{11}C , ^{11}B , ^{13}C , and ^{13}N , as explained in Ref. [49]. This method, however, is not practical for the space S_6 which comprises 21 s.p. levels. Therefore in this case the energies were derived in the way done in Ref. [51], while the pairing strengths were

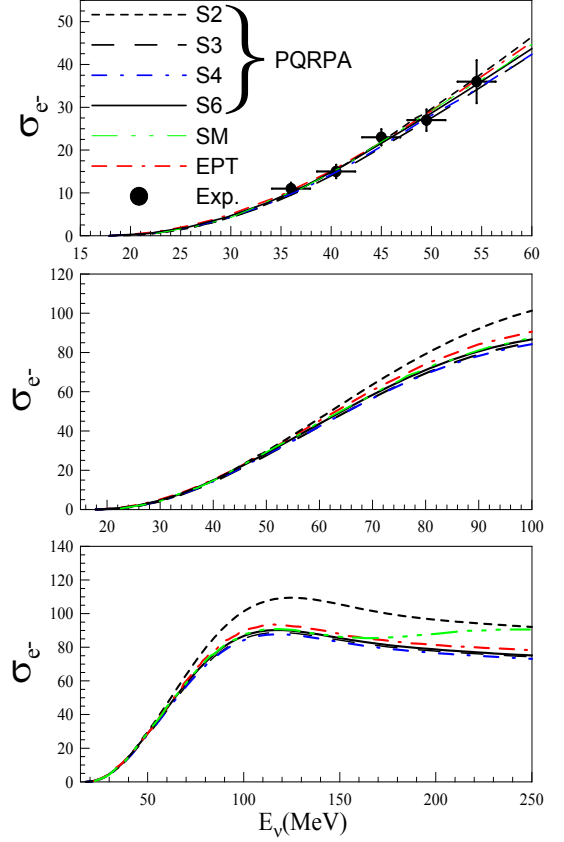


FIG. 3: (Color online) Same as in Figure 2, but now $t = 0$ for S_2 , and S_3 , $t = 0.2$ for S_4 , and $t = 0.3$ for S_6 . The SM, and EPT calculations are, respectively, from Refs. [98], and [16]. The experimental data in the DAR region are from Ref. [25].

adjusted to reproduce the experimental gaps in ^{12}C [89], considering all the quasiparticle energies up to 100 MeV.

For the purpose of the present study, we also employ the RQRPA theoretical framework [90]. In this case the ground state is calculated in the Relativistic Hartree-Bogoliubov model (RHB) using effective Lagrangians with density dependent meson-nucleon couplings and DD-ME2 parameterization [91], and pairing correlations are described by the finite range Gogny force [92]. Details of the formalism can be found in Refs. [93, 94]. The RHB equations, and respective equations for mesons are usually solved by expanding the Dirac spinors and the meson fields in a spherical harmonic oscillator basis with S_{20} s.p. space. In the present study of neutrino-nucleus cross sections, with energies of incoming neutrinos up to 600 MeV, we extend the number of oscillator shells up to $N = 30$ in order to accommodate s.p. states at higher energies necessary for description of cross sections involving higher energies of incoming (anti)neutrinos. The number of $2qp$ configurations in the RQRPA is constrained by the maximal excitation energy E_{2qp} . Within the RHB+RQRPA framework the oscillator basis is used only in RHB to determine the ground state and single-particle spectra.

The resulting wave functions are converted to coordinate space for evaluation of the RQRPA matrix elements. However, it is the original HO basis employed in RHB that determines the maximal E_{2qp} and the size of RQRPA configuration space.

A. Weak interaction properties of ^{12}N and ^{12}B ground states

Let us first compare the QRPA and PQRPA within the smallest configuration space S_2 , which contains 16 $J^\pi = 1^+$ states, and with null pp coupling: $t = 0$. The PQRPA ground state energies in ^{12}N , and ^{12}B , are, respectively: $\omega_{+1}(1^+) = 18.319$ MeV, and $\omega_{-1}(1^+) = 12.528$ MeV, while the corresponding wave functions read

$$\begin{aligned} |^{12}\text{N}\rangle &= 0.963|1p_{3/2}^\pi 1p_{1/2}^\nu\rangle + 0.232|1p_{3/2}^\pi 1p_{3/2}^\nu\rangle \\ &+ 0.122|1p_{1/2}^\pi 1p_{3/2}^\nu\rangle + 0.105|1p_{1/2}^\pi 1p_{1/2}^\nu\rangle \\ &+ \dots, \end{aligned} \quad (3.1)$$

and

$$\begin{aligned} |^{12}\text{B}\rangle &= -0.971|1p_{1/2}^\pi 1p_{3/2}^\nu\rangle + 0.204|1p_{3/2}^\pi 1p_{3/2}^\nu\rangle \\ &- 0.125|1p_{3/2}^\pi 1p_{1/2}^\nu\rangle + 0.090|1p_{1/2}^\pi 1p_{1/2}^\nu\rangle \\ &+ \dots \end{aligned} \quad (3.2)$$

The analogous QRPA energies are quite similar: $\omega_{+1}(1^+) = 17.992$ MeV, $\omega_{-1}(1^+) = 12.437$ MeV. However, the wave functions are quite different. The main difference is in the fact that QRPA furnishes the same wave functions for all four nuclei ^{12}N , ^{10}B , ^{14}N , and ^{12}B , being that of the ground state:

$$\begin{aligned} |1_{GS}^+\rangle &= -0.272|1p_{3/2}^\pi 1p_{1/2}^\nu\rangle - 0.759|1p_{3/2}^\pi 1p_{3/2}^\nu\rangle \\ &+ 0.356|1p_{1/2}^\pi 1p_{3/2}^\nu\rangle - 0.472|1p_{1/2}^\pi 1p_{1/2}^\nu\rangle \\ &+ \dots \end{aligned} \quad (3.3)$$

The difference in the wave functions is an important issue that clearly signals towards the need for the number projection. In fact, the PQRPA yields the correct limits ($1p_{3/2}^\pi \rightarrow 1p_{1/2}^\nu$ and $1p_{3/2}^\nu \rightarrow 1p_{1/2}^\pi$) for one-particle-one-hole (1p1h) excitations on the ^{12}C ground state to reach the ^{12}N , and ^{12}B nuclei. All remaining configurations in (3.1), and (3.2) come from the higher order 2p2h, and 3p3h excitations. Contrary, the QRPA state (3.3) is dominantly the two-hole excitation $[(1p_{3/2}^\pi)^{-1}, (1p_{3/2}^\nu)^{-1}]$, which corresponds to the ground state of ^{10}B . More details on this question can be found in Figure 3 of Ref. [49]. The 1p1h amplitudes $[(1p_{3/2}^\pi)^{-1}, 1p_{1/2}^\nu]$, and $[(1p_{3/2}^\nu)^{-1}, (1p_{1/2}^\pi)]$ are dominantly present in the following QRPA states

$$\begin{aligned} |1_2^+\rangle &= 0.708|1p_{1/2}^\pi 1p_{3/2}^\nu\rangle + 0.703|1p_{3/2}^\pi 1p_{1/2}^\nu\rangle \\ &+ \dots \\ |1_4^+\rangle &= -0.476|1p_{3/2}^\pi 1p_{1/2}^\nu\rangle + 0.437|1p_{3/2}^\pi 1p_{3/2}^\nu\rangle \\ &+ 0.441|1p_{1/2}^\pi 1p_{3/2}^\nu\rangle - 0.096|1p_{1/2}^\pi 1p_{1/2}^\nu\rangle \\ &+ \dots \end{aligned} \quad (3.4)$$

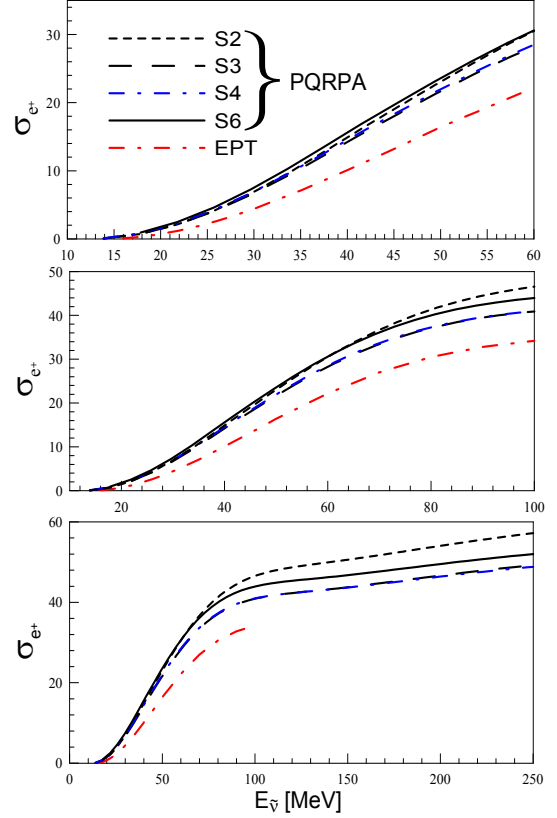


FIG. 4: (Color online) The calculated $^{12}\text{C}(\bar{\nu}, e^+)^{12}\text{B}$ cross-section $\sigma_{e^+}(E_{\bar{\nu}}, 1_1^+)$ (in units of 10^{-42} cm 2), plotted as a function of the incident antineutrino energy $E_{\bar{\nu}}$. Same as in Figure 3, the value of t is 0 for the s.p. spaces S_2 , and S_3 , 0.2 for S_4 and 0.3 for S_6 . The EPT calculation from Ref. [16] is also shown.

The wave functions displayed above clearly evidence the superiority of the PQRPA on the QRPA. Therefore from now on only the PQRPA results will be discussed for the exclusive observables.

In Figure 1 we show the ^{12}B and ^{12}N ground state energies, and the corresponding GT B -values within the PQRPA for different s.p. spaces, as function of the pp -coupling t . One sees that the energies depend rather weakly on both, and agree fairly well with the measured energies: $E(^{12}\text{B}) = 13.37$ MeV, and $E(^{12}\text{N}) = 17.33$ MeV [95], although the first one is somewhat underestimated, while the second one is somewhat overestimated. Both GT B -values significantly increase with t and diminish when size of the s.p. space is increased. For spaces S_2 and S_3 the best overall agreement with data ($B(^{12}\text{B}) = 0.466$, and $B(^{12}\text{N}) = 0.526$ [96]) is achieved with $t = 0$, while for spaces S_4 and S_6 this happens when the couplings are, respectively, $t = 0.2$, and $t = 0.3$.

After establishing the PQRPA parametrization, we analyze the behavior of the ECSs of the ground states in ^{12}N and ^{12}B , as a function of the size of the configura-

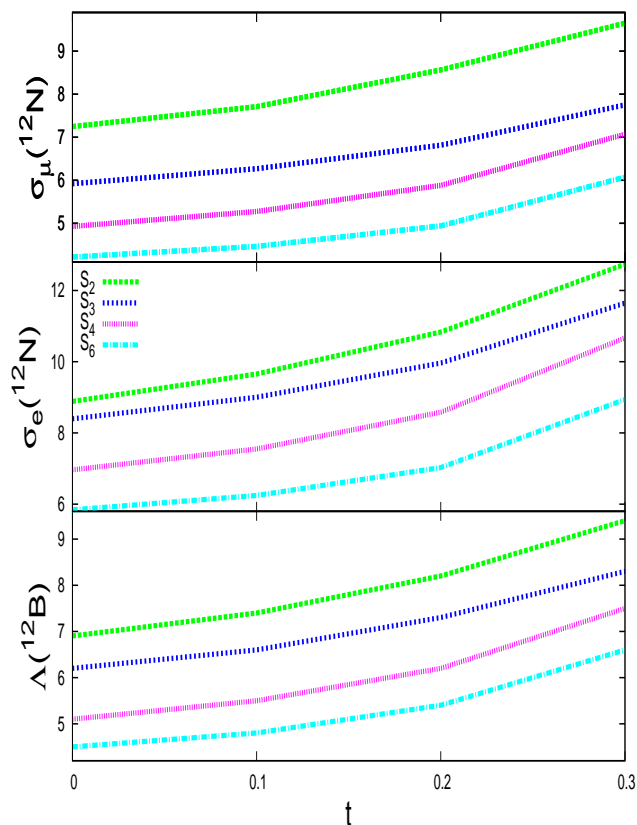


FIG. 5: (Color online) Muon capture transition rate to the ^{12}B ground state in units of $10^2 s^{-1}$, and electron and muon folded ECSs to the ^{12}N ground state in units of 10^{-42} cm^2 and 10^{-41} cm^2 , respectively. The experimental values, in above units, are: $\Lambda(^{12}\text{B}) = 6.2 \pm 0.3$ [45], $\bar{\sigma}_e(^{12}\text{N}) = 9.1 \pm 0.4 \pm 0.9$ [25], and $\bar{\sigma}_e(^{12}\text{N}) = 8.9 \pm 0.3 \pm 0.9$ [26], and $\bar{\sigma}_\mu(^{12}\text{N}) = 6.6 \pm 1.0 \pm 1.0$ [28], and $\bar{\sigma}_\mu(^{12}\text{N}) = 5.6 \pm 0.8 \pm 1.0$ [29].

tion space. Figure 2 shows the ECSs for the reaction $^{12}\text{C}(\nu, e^-)^{12}\text{N}$ (in units of 10^{-42} cm^2) for several configuration spaces, and for $t = 0$, within three different energy intervals. The top panel represents the DAR region, where experimental data are available [25], and search for neutrino oscillations was done [25, 27]. The middle panel represents the region of interest for supernovae neutrinos, as pointed out in Refs. [15, 97], while the bottom panel shows the asymptotic behavior of the cross-section, which becomes almost constant for $E_\nu \simeq 200 \text{ MeV}$. Within the spaces S_2 and S_3 the calculations reproduce quite well the experimental cross sections in the DAR region, as seen from the first panel.

In Figure 3 we show the calculated ECSs for the reaction $^{12}\text{C}(\nu, e^-)^{12}\text{N}$ within several configuration spaces, but now with different values of the pp -coupling. From comparison with the experimental data in the DAR region [25] one observes that the appropriate values for the coupling t for s.p. spaces S_4 , and S_6 , are, respectively, $t = 0.2$, and $t = 0.3$, i.e., the same as those required to reproduce the experimental energies and the GR B -values in ^{12}B , and ^{12}N .

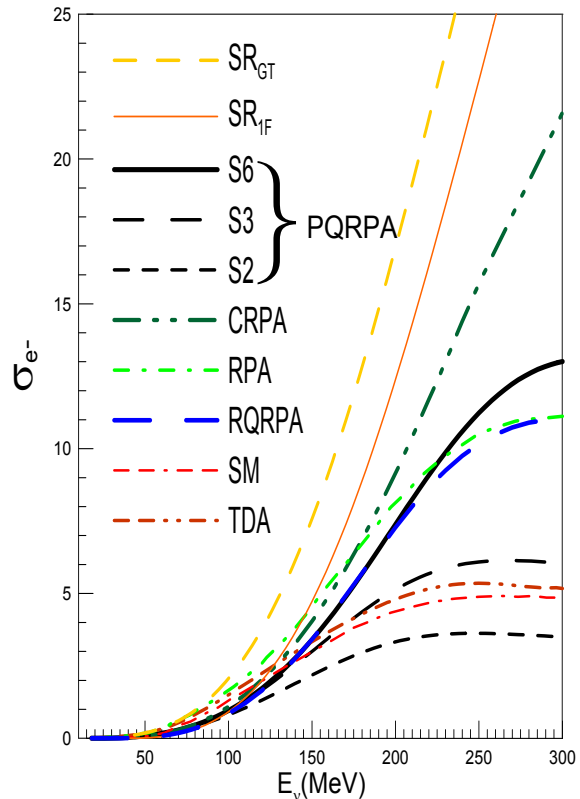


FIG. 6: (Color online) Inclusive $^{12}\text{C}(\nu, e^-)^{12}\text{N}$ cross-section $\sigma_{e^-}(E_\nu)$ (in units of 10^{-39} cm^2) plotted as a function of the incident neutrino energy E_ν . The PQRPA results within the s.p. spaces S_2 , S_3 , and S_6 , and the same values of $s = t$ as in Figure 3, are compared with two sum rule limits (as explained in the text): SR_{GT} , and SR_{1F} obtained with average excitation energy $\bar{\omega}_{J_n^\pi}$ of 17.34, and 42 MeV, respectively. Several previous RPA-like calculations, namely: RPA [43], CRPA [102], and RQRPA within S_{20} for $E_{2qp}=100 \text{ MeV}$ [51], as well as the SM [43], and the TDA [34] are also shown.

This change of parametrization hint at the self-consistency of the PQRPA, and comes from the fact that in this model: i) the GT strength allocated in the ground state is moved to another 1^+ states when the size of the space is increased, and ii) the effect of the pp residual interaction goes in the opposite direction, returning the GT strength to the 1_1^+ state. Only for the space S_2 the cross-section $\sigma_{e^-}(E_\nu, 1_1^+)$ is appreciable larger (at $E_\nu \gtrsim 60 \text{ MeV}$) than for other spaces, which is just because of the small number of configurations in this case. In the same figure are exhibited as well the results for the ECSs evaluated within the SM [98], and the EPT [16]. Both of them agree well with the data and with the present calculation.

The results for the reaction $(\bar{\nu}, e^+)$ to the ground state in ^{12}B are shown in Figure 4. The cross-section $\sigma_{e^+}(E_{\bar{\nu}}, 1_1^+)$ is similar to that produced by neutrinos but significantly smaller in magnitude. When compared with

the EPT result [16], which are also shown in the same figure, one notices that they are considerable different. To some extent this is surprising as in the case of neutrinos the two models yield very similar results. One should remember that in the EPT model the axial form factor, used for both neutrinos and antineutrinos, is gauged to the average of the GR B -values in ^{12}B , and ^{12}N , which, in turn, are well reproduced by the PQRPA. Therefore it is difficult to understand why the EPT results agree with the present calculations for neutrinos and disagree for antineutrinos.

In Figure 5 we show the dependence on the configuration space of the exclusive muon capture transition rate $\Lambda(1_1^+)$ to the ^{12}B ground state, and the electron and muon flux-averaged ECSs, given by (2.28), to the ^{12}N ground state, i.e., $\bar{\sigma}_e(1_1^+)$, and $\bar{\sigma}_\mu(1_1^+)$. As in Refs. [48, 49] the electron neutrino distribution $n_e(E_\nu)$ was approximated with the Michel energy spectrum [9, 99], and for the muon neutrinos we used $n_\mu(E_\nu)$ from Ref. [30]. The energy integration is carried out in the DAR interval $m_e + \omega_{J_f} \leq \Delta_{J_f}^{\text{DAR}} \leq 52.8$ MeV for electrons and in the DIF interval $m_\mu + \omega_{J_f} \leq \Delta_{J_f}^{\text{DIF}} \leq 300$ MeV for muons. From Figure 5, and comparison with experimental data:

$$\begin{aligned} \Lambda(^{12}\text{B}) &= 6.2 \pm 0.3 [45], \\ \bar{\sigma}_e(^{12}\text{N}) &= 9.1 \pm 0.4 \pm 0.9 [25], 8.9 \pm 0.3 \pm 0.9 [26], \\ \bar{\sigma}_\mu(^{12}\text{N}) &= 6.6 \pm 1.0 \pm 1.0 [28], 5.6 \pm 0.8 \pm 1.0 [29], \end{aligned}$$

one finds out, as for results shown in Figures 1, and 3, the model self-consistency between s.p. spaces and the pp -couplings. That is, for larger s.p. spaces larger values of t are required. In brief, the experimental data of $\bar{\sigma}_e(^{12}\text{N})$, and $\bar{\sigma}_\mu(^{12}\text{N})$ are well reproduced by the PQRPA. The same is true for the SM calculations [42, 43], while in RPA, and QRPA models they are strongly overestimated, as can be seen from Table II in Ref. [43], and Table 1 in Ref. [50].

B. Inclusive cross-sections $^{12}\text{C}(\nu, e^-)^{12}\text{N}$ and $^{12}\text{C}(\bar{\nu}, e^+)^{12}\text{B}$, and Sum Rule

In Figure 6 we confront the PQRPA results for the ICS $\sigma_{e^-}(E_\nu)$ within spaces S_2 , S_3 , and S_6 with the corresponding sum-rules $\sigma_{e^-}^{SR}(E_\nu)$ evaluated from (B1). One immediately sees that the PQRPA results depend very strongly on the size of the employed s.p. space. On the other hand, as already mentioned in the Appendix B, the sum rule $\sigma_{e^-}^{SR}(E_\nu)$ depends on the average energy $\overline{\omega_{J_\pi}}$. Here we use two values $\overline{\omega_{J_\pi}} = 17.34$ MeV, which is the ground state energy ^{12}N , (GT-resonance), and $\overline{\omega_{J_\pi}} = 42$ MeV, which is roughly the energy of the first forbidden resonance [100]. The corresponding curves in Figure 6 are labeled, respectively, as SR_{GT} , and SR_{1F} . They should be the upper limits for allowed and first forbidden transitions, respectively. The validity of these sum rules is questionable for neutrinos energies of several hundred MeV, as already pointed out by Kuramoto *et al.* [74]. In

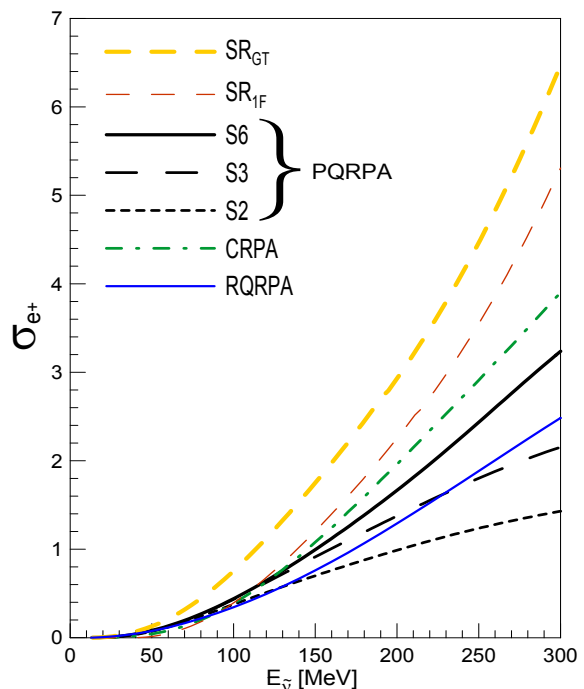


FIG. 7: (Color online) Inclusive $^{12}\text{C}(\bar{\nu}, e^+)^{12}\text{B}$ cross-section $\sigma_{e^+}(E_\nu)$ (in units of 10^{-39} cm^2) plotted as a function of the incident neutrino energy E_ν . All results were obtained in the same way as in the neutrino case in Figure 6.

fact, we note that the cross section SR_{GT} (SR_{1F}) exceeds the free particle cross section $\sigma_6 \equiv 6\sigma(\nu_e + n \rightarrow e^- + p)$ for $E_\nu > 200$ MeV ($E_\nu > 300$ MeV) [101].

Several previous SM and RPA-like calculations of $\sigma_{e^-}(E_\nu)$, employing different effective axial-vector coupling constants, and different s.p. spaces, are exhibited in Figure 6 as well, namely:

- TDA [34], with $g_A = 1.23$, and S_2 ,
- SM and RPA [43], with $g_A = 0.88$, and S_3 ,
- CRPA [102], with $g_A = 1.26$, and S_4 ,
- RQRPA [51], with $g_A = 1.23$, S_{20} , and $E_{2qp}=100$ MeV.

It is important to specify the values g_A because the partial cross sections are predominantly of the axial-vector type (specially the allowed ones), which are proportional to g_A^2 . In spite of very significant differences in g_A , and the s.p. spaces, the different calculations of $\sigma_{e^-}(E_\nu)$ yield quite similar results for energies $E_\nu \lesssim 130$ MeV, lying basically in vicinity of the the sum-rule result SR_{1F} . But for higher energies they could become quite different, and are clearly separated in two groups at $E_\nu = 300$ MeV. In the first group with $\sigma_{e^-}(E_\nu) \lesssim 5 \times 10^{-39}$ cm^2 are: the SM, TDA, and PQRPA within spaces S_2 , S_3 , while in the second one with $\sigma_{e^-}(E_\nu) \gtrsim 10 \times 10^{-39}$ cm^2 are: the RPA, RQRPA, CRPA and PQRPA within space S_6 . Volpe *et al.* [43] have found that the difference between their SM and RPA calculations is due to differences in the correlations taken into account, and to a too small SM space. We also note that only the CRPA result approaches the sum rule limits for $E_\nu > 200$ MeV.

Similar results for the inclusive $^{12}\text{C}(\bar{\nu}, e^+)^{12}\text{B}$ cross-

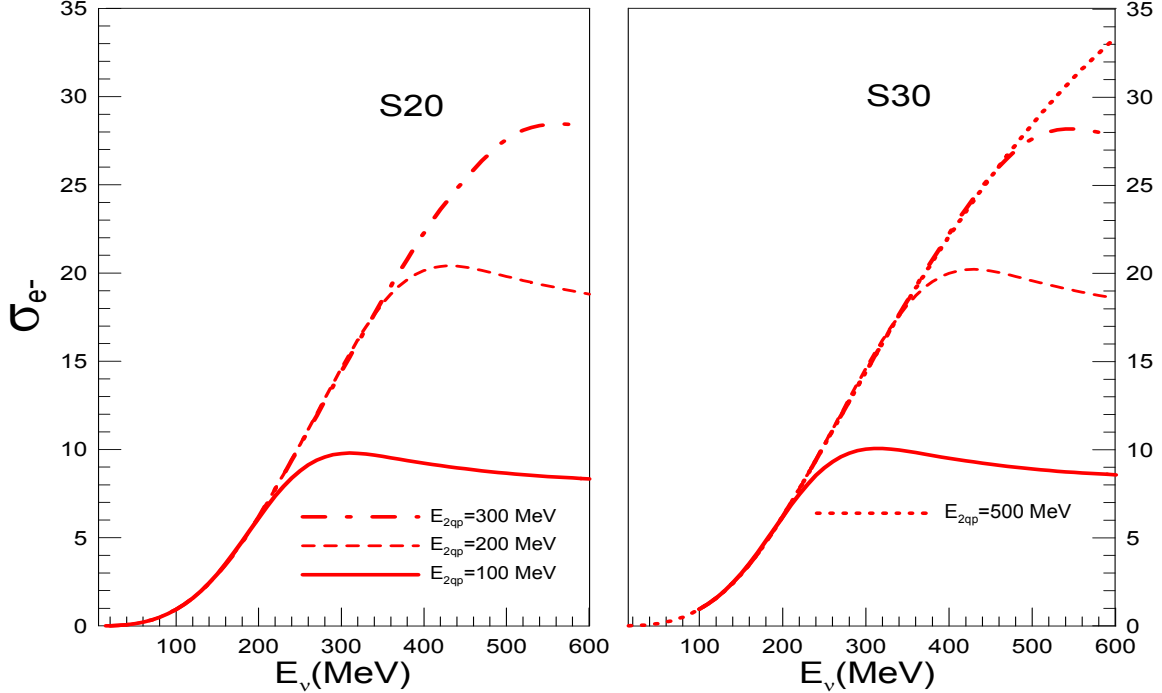


FIG. 8: (Color online) Inclusive $^{12}\text{C}(\nu, e^-)^{12}\text{N}$ cross-section $\sigma_{e^-}(E_\nu)$ (in units of 10^{-39} cm^2) plotted as a function of the incident neutrino energy E_ν , evaluated in RQRPA with different configuration spaces. These cross sections are plotted as functions of the incident neutrino energy with different cut-off of the E_{2qp} quasiparticle energy as it is explained in the text. The left and right panels show the cross section evaluated with S_{20} , and S_{30} s.p. spaces. The last cross section shows that the convergence of the calculation is achieved up to 600 MeV of incident neutrino energy.

section $\sigma_{e^+}(E_{\bar{\nu}})$ are displayed in Figure 7, and analogous comments can be done here. For the comparison, we show in the figure the antineutrino- ^{12}C cross-sections evaluated with the CRPA [102].

C. Large configuration spaces

As there are no experimental data on flux unfolded ICSs for $E_\nu \leq 400$ MeV we cannot conclude which of the results displayed in Figures 6, and 7 are good and which are not. We can only conclude that the ICSs strongly depend on the size of the s.p. space. In the PQRPA calculations we are not able to use spaces larger than S_6 because of numerical difficulties. Thus instead of using the PQRPA, from now on we employ the RQRPA where such calculations are feasible. It is important to note that within the RHB+RQRPA model the oscillator basis is used only in the RHB calculation in order to determine the ground state and the single-particle spectra. The wave functions employed in RPA equations are obtained by converting the original HO basis to the coordinate representation. Therefore, the size of the RQRPA configuration space and $2qp$ energy cut-offs are determined by the number of oscillator shells in the RHB model.

First, we analyze the effect of the cut-off energy within the S_{20} space on $\sigma_{e^-}(E_\nu)$ for E_ν up to 600 MeV. From

the left panel in Figure 8 one sees that at high energies this cross-section increases roughly by a factor of two when E_{2qp} is augmented from 100 to 200 MeV. The increase of the cross-section is also quite important when E_{2qp} is moved from 200 to 300 MeV. For the limiting value of $E_{2qp}=300$ MeV, all possible configurations are included in RQRPA calculations. Next, we do the same within the S_{30} space, and the resulting $\sigma_{e^-}(E_\nu)$ are displayed on the right panel of Figure 8. From the comparison of both panels it is easy to figure out that up to $E_{2qp} = 300$ MeV the cross sections obtained with the S_{30} space are basically the same to those calculated with the S_{20} space. Small differences between the cross sections using S_{20} and S_{30} spaces for E_{2qp} up to 300 MeV are caused by modifications of positive-energy single-particle states contributing to the QRPA configuration space within the restricted $2qp$ energy window. But, for $E_\nu \gtrsim 400$ MeV additional transition strength appears in the S_{30} space when E_{2qp} is moved up to 400 MeV, from where further increase in E_{2qp} has a very small effect. We conclude therefore that the configuration space engendered by $N = 20$ HO shells with $E_{2qp} = 300$ MeV, is large enough to describe $\sigma_{e^-}(E_\nu)$ with E_ν up to 400 MeV. Similarly, the space brought about by $N = 30$ HO shells with $E_{2qp} = 400$ MeV is appropriate to account for $\sigma_{e^-}(E_\nu)$ up to $E_\nu = 600$ MeV. For larger neutrino energies very likely we would have to continue increasing

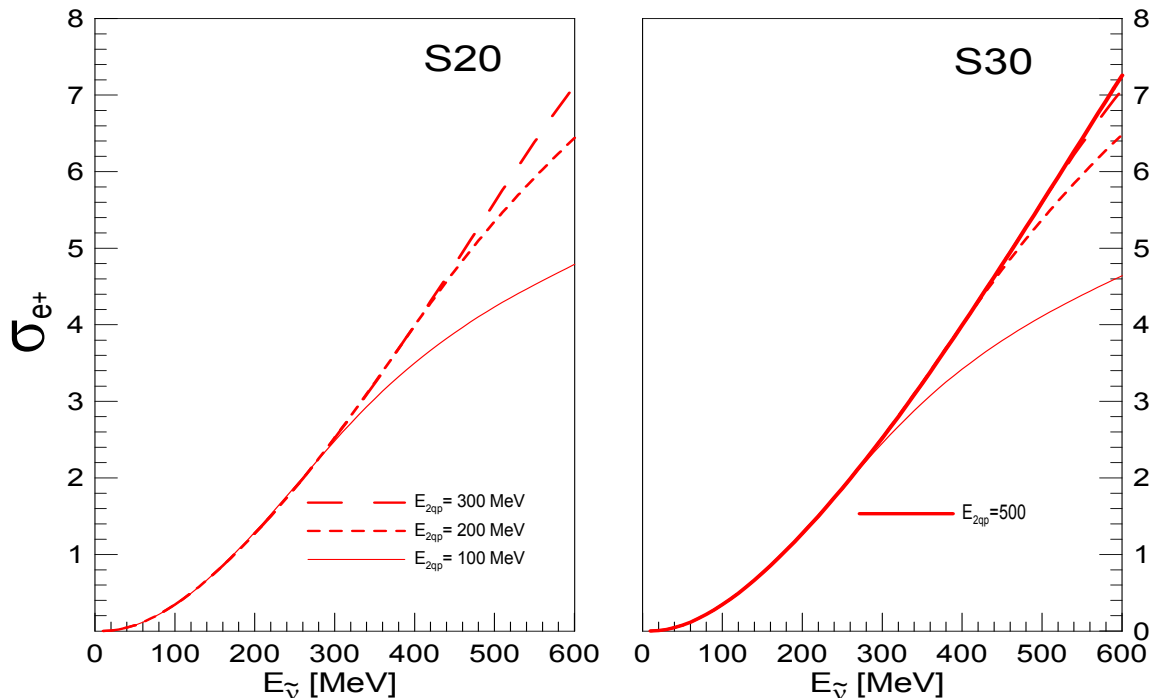


FIG. 9: (Color online) Same as in Figure 8 but for the $^{12}\text{C}(\bar{\nu}, e^+)^{12}\text{B}$ cross-section $\sigma_{e^+}(E_{\bar{\nu}})$.

the number of shells.

Analogous results for antineutrino ICSs $\sigma_{e^+}(E_{\bar{\nu}})$ are displayed in Figure 9. One notes important differences in comparison with $\sigma_{e^-}(E_{\nu})$ shown in Figure 8. First, here the spaces S_{20} and S_{30} yield almost identical results in the entire interval of antineutrino energies up to $E_{\bar{\nu}} = 600$ MeV. Second, the successive increase in the cross-sections when the cut-off E_{2qp} is augmented in steps of 100 MeV are smaller, and decrease more rapidly than in the neutrino case. This suggests that the configuration space is now sufficiently large to appropriately account for $\sigma_{e^+}(E_{\bar{\nu}})$ even at antineutrino energies larger than 600 MeV.

At present, due to numerical difficulties, we cannot perform the RQRPA calculations for the full range of neutrino energies where the QE cross section was measured at MiniBooNE [13], but only up to 0.6 GeV. However, we feel that it could still be illustrative for comparison with data. This is done in Figure 10, which is basically a piece of Figure 21 Ref. [73] for the QE $\sigma_{\mu^-}(E_{\nu})$ (see also Ref. [103]), where is incorporated our result for $\sigma_{e^-}(E_{\nu})$ from Figure 8 for S_{30} and $E_{2qp} = 500$ MeV. As already pointed out in the Introduction, at relatively high energies ($E_{\nu} > 300$ MeV) the electron and muon neutrino cross sections converge to each other, and therefore, in the present analysis, the electron neutrino cross section provides a reasonable upper limit estimate. One sees that we underestimate the data by almost a factor of two. But one should keep in mind that, while we use $g_A = 1$ (see (2.4)) in the RFGM calculation done by Martini *et al.* [73, 103] $g_A = 1.255$ was used. Be-

ing the axial-vector contribution dominant for the latter value of the coupling constant, one would have to renormalize our $\sigma_{e^-}(E_{\nu})$ by a factor ~ 1.5 . Such a result is also shown in Figure 10, and although the resulting cross section still underestimates somewhat the data for $\sigma_{\mu^-}(E_{\nu})$, it is notably superior to the pure 1p-1h result from Ref. [73], where good agreement with the data is achieved only after considering additional two-body (2p-2h) and three-body (3p3h) decay channels. One should keep in mind, however, that as the weak decay Hamiltonian is one-body operator, these excitations are only feasible via the ground-state correlations (GSC), which basically redistribute the 1p-1h transition strength without increasing its total magnitude when the initial wave function is properly normalized. In the present work, as well as in all SM-like calculations, the GSC, and a normalized initial state wave function are certainly considered to all orders in perturbation theory through the full diagonalization of the hamiltonian matrix. On the other hand, in Refs. [73, 103] the GSC are taken into account in second order perturbation theory, but there are no references to the normalization of the ^{12}C ground-state wave function. How to carry out the normalization in the framework of the infinite nuclear matter model is discussed in a recent paper related to the nonmesonic weak decay of the hypernucleus $^{12}_{\Lambda}\text{C}$ [104]; see also Refs. [105–107].

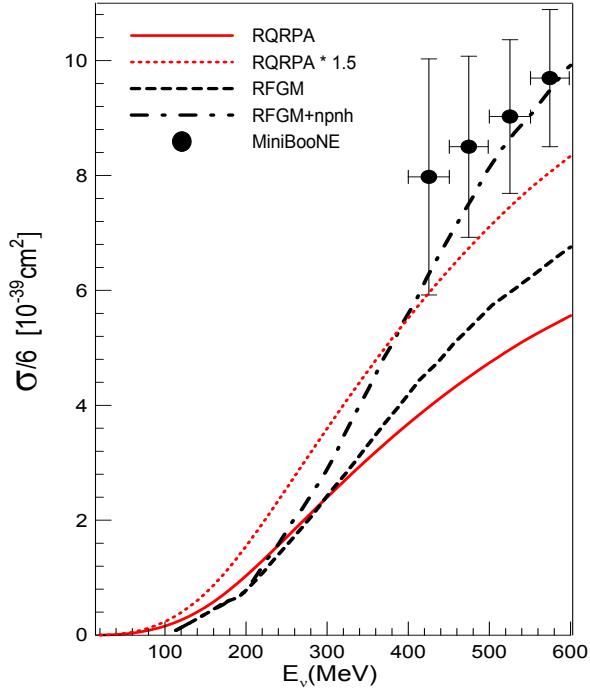


FIG. 10: (Color online) The calculated RQRPA (within S_{30} and $E_{2qp} = 500$ MeV) quasi-elastic ($\nu_e, {}^{12}\text{C}$) cross section per neutron (full line) is compared with that for the ($\nu_\mu, {}^{12}\text{C}$) scattering data measured at MiniBooNE [13]; with dotted line is shown the same calculation but renormalized by a factor 1.5. Also are displayed the calculations done by Martini *et al.* [73, 103] within the RFGM for pure (1p-1h) excitations (dashed line), and with the inclusion of the np-nh channels (dot-dashed line).

D. Multipole decomposition of cross-sections

We did not mention yet the contributions of different multipoles to the ICSs. Normally, the RHB model within S_{20} , and with $J^\pi \leq 7^\pm$, provides converged results for RQRPA excitation spectra at incident neutrino energies $E_\nu \leq 300$ MeV as seen from Figure 2 in Ref. [51]. But this is not the case for neutrino-nucleus cross sections at energies $E_\nu \gtrsim 300$ MeV where one has to consider large cutoff energies E_{2qp} . In fact, it is necessary to consider more and more multipoles according as the configuration space is enlarged by increasing E_{2qp} . This is illustrated in Figure 11 for the case of $E_{2qp} = 500$ MeV. One sees that are significant all multipoles up to $J^\pi = 14^\pm$ for neutrinos, and up to $J^\pi = 11^\pm$ for antineutrinos.

Next we discuss the partial multipole contributions to the ICS, having in view the degree of forbiddenness of the transition matrix elements, namely,

- Allowed: $\sigma_{e^+}^A(E_{\bar{\nu}})$, with $J^\pi = 0^+, 1^+$,
- First-forbidden $\sigma_{e^+}^{1F}(E_{\bar{\nu}})$, with $J^\pi = 0^-, 1^-, 2^-$,
- Second-forbidden $\sigma_{e^+}^{2F}(E_{\bar{\nu}})$, with $J^\pi = 2^+, 3^+$, and
- Third-forbidden $\sigma_{e^+}^{3F}(E_{\bar{\nu}})$ with $J^\pi = 3^-, 4^-$,

cross-sections. Thus, in the left panel of Figure 12 we show these individual contributions for the inclusive

${}^{12}\text{C}(\bar{\nu}, e^+){}^{12}\text{B}$ cross-section $\sigma_{e^+}(E_{\bar{\nu}})$, evaluated within both the PQRPA (spaces S_2 , and S_6) the RQRPA (space S_{30} with $E_{2qp} = 500$ MeV).

The same is done for the corresponding derivatives, i.e., the spectral functions $d\sigma_{e^+}(E_{\bar{\nu}})/dE_{\bar{\nu}}$, on the right panel of the same figure. Several conclusions can be drawn. First, as in the case of total $\sigma_{e^+}(E_{\bar{\nu}})$, they depend very strongly on the size of the configuration space. This dependence, in turn, increases with the degree of forbiddenness; that is, it is more pronounced for first-forbidden than for allowed transitions, and so on. Second, within the PQRPA the allowed cross-section $\sigma_{e^+}^A(E_{\bar{\nu}})$ exhibits a resonant pattern at low energy, and is dominant for $E_{\bar{\nu}} \lesssim 50$ MeV. For large s.p. spaces its contribution is quite significant even at $E_{\bar{\nu}} = 500$ MeV. ⁵ In the case of RQRPA, the spectral function $d\sigma_{e^+}^A(E_{\bar{\nu}})/dE_{\bar{\nu}}$ also displays low-energy resonant structure, and $\sigma_{e^+}^A(E_{\bar{\nu}})$ is always smaller in magnitude than in the PQRPA case. Third, $\sigma_{e^+}^{1F}(E_{\bar{\nu}})$ is peaked at $E_{\bar{\nu}} \sim 75$ MeV, and its contribution is always larger than that of $\sigma_{e^+}^A(E_{\bar{\nu}})$ for $E_{\bar{\nu}} \gtrsim 150$ MeV. Fourth, $\sigma_{e^+}^{2F}(E_{\bar{\nu}})$, and $\sigma_{e^+}^{3F}(E_{\bar{\nu}})$ mainly contribute in the interval $150 \lesssim E_{\bar{\nu}} \lesssim 400$ MeV, and their overall contributions are of the same order of magnitude, and comparable to that of the $\sigma_{e^+}^{1F}(E_{\bar{\nu}})$. Fifth, the contributions of the remaining multipoles with $J^\pi = 4^+, 5^\pm, 6^\pm, 7^\pm$ are always very small for the space S_2 , but are quite sizeable for S_6 at high energies. For instance, at $E_{\bar{\nu}} = 100, 300, 600$ MeV they contribute, respectively with 0.02%, 0.86%, 1.18% within the space S_2 , and 0.04%, 14%, 20% for S_6 . With further increase of the single-particle basis, configurations from higher multipoles become more pronounced at higher neutrino energies. In particular, the sum of contributions coming from $J^\pi = 4^+, \dots, 11^\pm$ multipoles when evaluated within the RQRPA using the space S_{30} and maximal value of $E_{2qp}=500$ MeV, are 1.1%, 14.4%, and 33.2% at $E_\nu=100, 300$, and 600 MeV, respectively.

Recently Lazauskas and Volpe [108, 109] have suggested the convenience of performing nuclear structure studies using low energy neutrino and antineutrino beams. Because of feasibility reasons the flux covers 80 MeV only. Nevertheless, from the analysis of ${}^{16}\text{O}$, ${}^{56}\text{Fe}$, ${}^{100}\text{Mo}$ and ${}^{208}\text{Pb}$ nuclei within the QRPA using the Skyrme force they were able to disentangle the multipole distributions of forbidden cross-sections, showing that the forbidden multipole contribution is different for various nuclei. In this work we extend this kind of study to ${}^{12}\text{C}$.

In Table I we show the results for the flux-averaged cross sections $\bar{\sigma}_{e^+}$ for the reaction ${}^{12}\text{C}(\bar{\nu}, e^+){}^{12}\text{B}$. In (2.29) we have used the same antineutrino fluxes $n_{e^+}(E_{\bar{\nu}})$

⁵ The denominations here don't have exactly the same meaning as in the low-energy β -decay, where allowed transitions are those within the same HO shell ($\Delta N = 0$), while here all values of ΔN are permitted. Similarly happens with the forbidden transitions. The degrees of hindrance basically come from value of the orbital angular momenta.

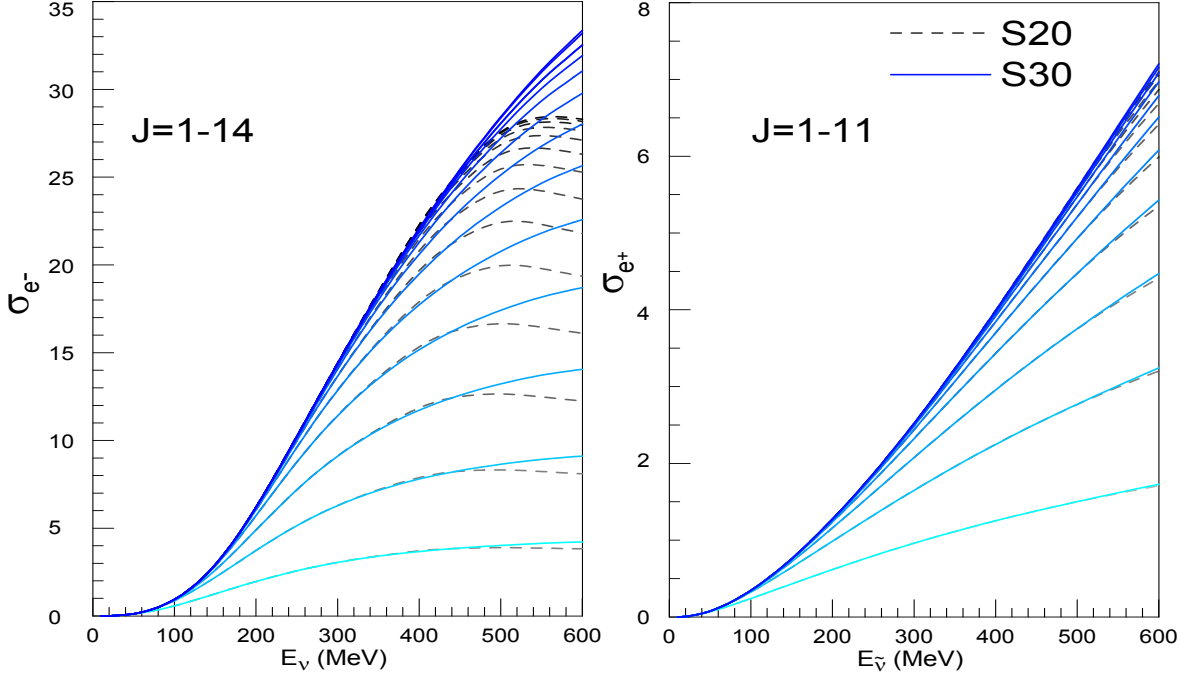


FIG. 11: (Color online) Left and right panels show, respectively, the cross sections $\sigma_{e^-}(E_\nu)$, and $\sigma_{e^+}(E_{\bar{\nu}})$ (in units of 10^{-39} cm^2) evaluated in RQRPA for S_{20} , and S_{30} s.p. spaces with the cutoff $E_{2qp} = 500$ MeV, and different maximal values of J^\pm , with J going from 1 up to 14 for neutrinos, and from 1 up to 11 for antineutrinos.

as in Ref. [108], i.e., the DAR flux, and those produced by boosted ${}^6\text{He}$ ions with different values of time dilation factor $\gamma = 1/\sqrt{1 - v^2/c^2}$. Results of two calculations are presented: i) PQRPA within S_6 , and ii) RQRPA within $N = 20$, and cutoff $E_{2qp} = 300$ MeV. One sees that in both models, and principally in the PQRPA, the allowed transitions dominate the forbidden one, and specially for the low-energy beam with $\gamma = 6$. The contributions of the second-forbidden processes are very small in all the cases, while those coming from third-forbidden ones are always negligible. All this is totally consistent with the results shown in Figure 12, from where it is clear that to study second and third forbidden reactions in ${}^{12}\text{C}$, one would need fluxes $n_{e^+}(E_{\bar{\nu}})$ with $E_{\bar{\nu}}$ at least up to $\gtrsim 150$ MeV. It should also be stressed that our results both for allowed and forbidden transitions fully agree with those obtained in Ref. [108]; the difference in ${}^{16}\text{O}$ comes from the double-shell closure in this nucleus.

E. Supernova neutrinos

We also address briefly the $\nu/\bar{\nu}$ - ${}^{12}\text{C}$ nucleus cross-sections related with astrophysical applications, the knowledge of which could have important implications. For this purpose, are evaluated the $\bar{\sigma}_{e^\pm}$ folded with supernovae $\nu/\bar{\nu}$ spectra represented by a normalized Fermi-Dirac distribution with temperatures in the interval $T_{\nu_e} = 2 - 12$ MeV, which includes the most commonly

TABLE I: Fraction (in %) of flux-averaged cross sections $\bar{\sigma}_{e^+}$ for ${}^{12}\text{C}(\bar{\nu}, e^+){}^{12}\text{B}$ for allowed (A), first-forbidden (1F), second-forbidden (2F), and third-forbidden (3F) processes. The antineutrino fluxes $n_{e^+}(E_{\bar{\nu}})$ are the same as in Ref. [108], i.e., the DAR flux, and those produced by boosted ${}^6\text{He}$ ions with different values of $\gamma = 1/\sqrt{1 - v^2/c^2}$. Results of two calculations are presented: i) PQRPA within S_5 , and ii) RQRPA within $N = 30$, and cutoff $E_{2qp} = 300$ MeV.

	DAR	γ		
		6	10	14
A				
PQRPA	79.43	92.09	77.00	63.01
RQRPA	84.40	94.88	82.25	67.15
1F				
PQRPA	20.03	7.83	22.16	33.76
RQRPA	15.10	4.13	16.86	29.61
2F				
PQRPA	0.51	0.07	0.78	2.89
RQRPA	0.55	0.08	0.81	2.91
3F				
PQRPA	0.018	0.002	0.04	0.33
RQRPA	0.025	0.011	0.05	0.33

used values are $T_{\nu_e} = 3.2$ MeV and $T_{\bar{\nu}_e} = 5.0$ MeV. For mean energies $\langle E_\nu \rangle \approx 3.15 \times T_\nu$, and zero chemical potential [110, 111] the neutrino flux is

$$n_e(E_\nu) = \frac{0.5546}{T_\nu^3} \frac{E_\nu^2}{e^{E_\nu/T_\nu} + 1}, \quad (3.5)$$

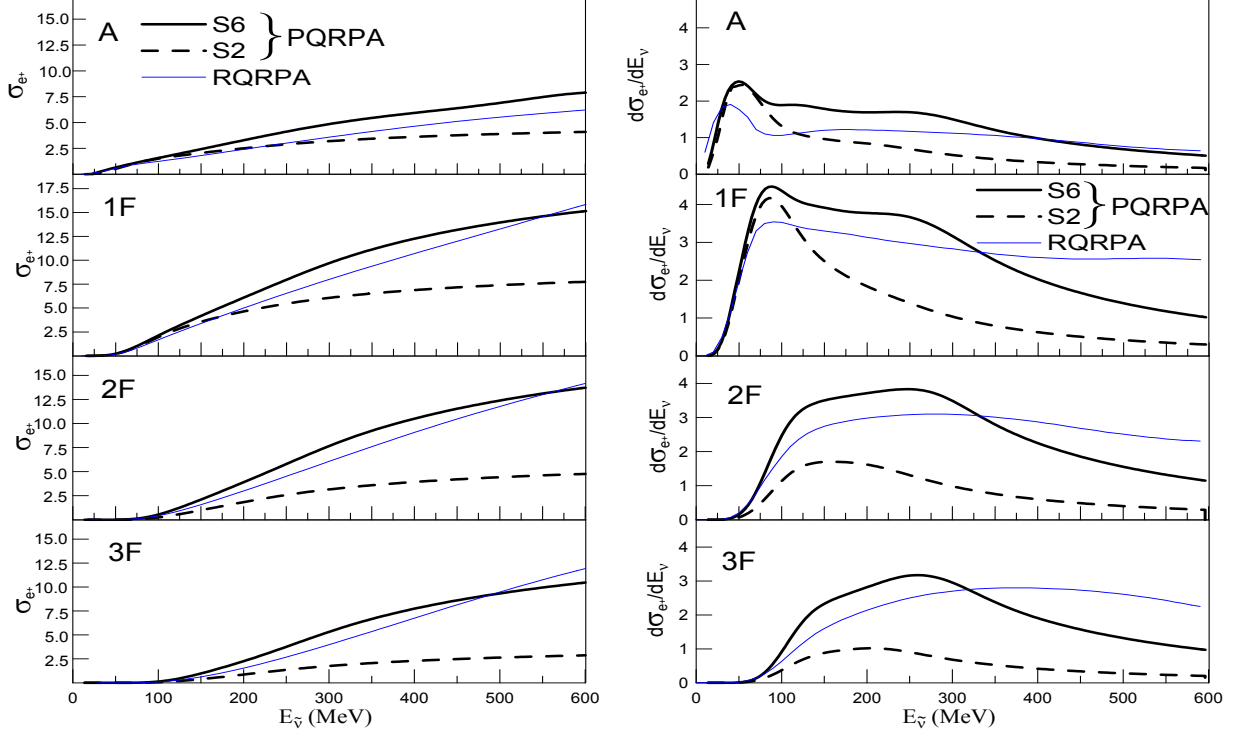


FIG. 12: (Color online) Left panel: Allowed ($J^\pi = 0^+, 1^+$), first-forbidden ($J^\pi = 0^-, 1^-, 2^-$), second-forbidden ($J^\pi = 2^+, 3^+$), and third-forbidden ($J^\pi = 3^-, 4^-$) inclusive $^{12}\text{C}(\bar{\nu}, e^+)^{12}\text{B}$ cross-section $\sigma_{e^+}(E_{\bar{\nu}})$ (in units of 10^{-42} cm^2), plotted as a function of the incident neutrino energy $E_{\bar{\nu}}$. Right panel: Same as left panel but now for $d\sigma_{e^+}(E_{\bar{\nu}})/dE_{\bar{\nu}}$ (in units of $10^{-42} \text{ cm}^2 \text{ MeV}^{-1}$).

and similarly for antineutrinos. For the sake of simplicity we do not analyze same relevant aspects of $n_e(E_\nu)$ in supernova simulation, such as the MSW effect (see, for example, Ref. [112]), and the spectral swapping of the neutrino flux (Ref. [113]). In Figure 13 we confront the ν - ^{12}C cross sections averaged over supernova ν -fluxes for the range of $T_\nu = 2 - 12 \text{ MeV}$, obtained within following calculations:

- i) PQRPA within S_6 ,
- ii) RQRPA within S_{30} and $E_{2qp} = 500 \text{ MeV}$, and
- iii) SM done by Suzuki *et al.* [44] with the SFO Hamiltonian (the PSDMK2 interaction yields a quite similar result).

As seen from Figure 13, in the vicinity of the temperatures mentioned at the beginning ($T_\nu = 3 - 5 \text{ MeV}$), these three calculations yield, respectively, that: i) $\bar{\sigma}_{e^+}$ is significantly larger than $\bar{\sigma}_{e^-}$, ii) $\bar{\sigma}_{e^-}$ is only slightly larger than $\bar{\sigma}_{e^+}$, and iii) $\bar{\sigma}_{e^+} \cong \bar{\sigma}_{e^-}$. Both SM cross sections are always smaller than those obtained in the other two calculations, and specially in comparison with the RQRPA one.

IV. SUMMARY AND CONCLUDING REMARKS

The present work is a continuation of our previous works [48, 49]. In fact, the formalism for weak interaction processes introduced there is now elaborated more thoroughly yielding very simple expressions for the transition rates, which greatly facilitate the numerical calculation. This is done through the separation of the nuclear matrix elements into their real and imaginary parts, which, in turn, permits to split the transition rates, for neutrino-nucleus reactions (2.22) into natural (A6) and unnatural parity (A7) operators. Similar separation is done for the muon capture transition rate (D3) in Eqs. (D4) and (D5). Moreover, consequences of explicit violation of CVC hypothesis by the Coulomb field (2.18) are addressed for the first time, and the sum rule approach for the inclusive cross section, proper to the present formalism, has been worked out in the Appendix B. For the sake of completeness, the extreme relativistic limit of neutrino-nucleus cross section is also presented in the Appendix C, where in the formula for transition rates turn out to be still simpler. We note that, except at very low neutrino energies, they can be used without any restriction in practical applications.

We have discussed in details the inclusive properties

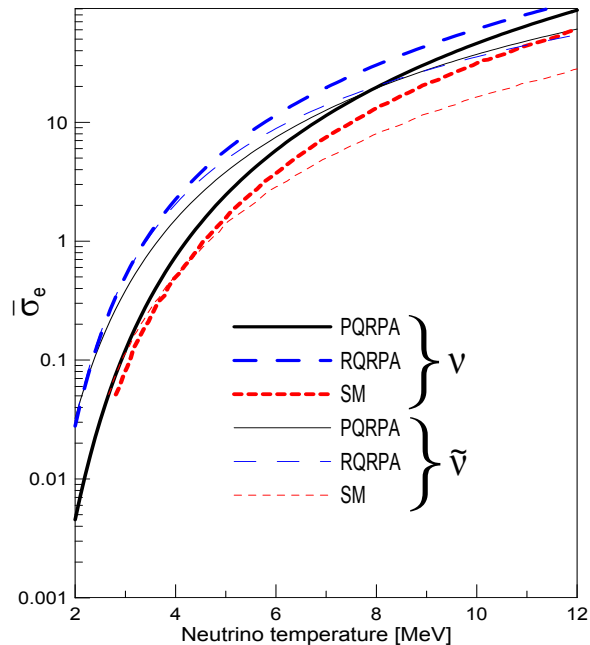


FIG. 13: (Color online) Flux-averaged neutrino and antineutrino cross sections $\bar{\sigma}_{e\pm}$ in ^{12}C with typical supernovae fluxes.

that comprise:

- i) Ground state energies in ^{12}B and ^{12}N , and the corresponding GT B -values (Figure 1),
- ii) Exclusive $^{12}\text{C}(\nu, e^-)^{12}\text{N}$ cross-section $\sigma_e(E_\nu, 1_1^+)$, as a function of the incident neutrino energy E_ν (Figures 2, and 3),
- iii) Exclusive $^{12}\text{C}(\bar{\nu}, e^+)^{12}\text{B}$ cross-section $\sigma_{e^+}(E_{\bar{\nu}}, 1_1^+)$, as a function of the incident antineutrino energy $E_{\bar{\nu}}$ (Figure 4), and
- iv) Muon capture transition rate to the ^{12}B ground state, and electron and muon folded cross-sections to the ^{12}N ground state $\bar{\sigma}_e(1_1^+)$, and $\bar{\sigma}_\mu(1_1^+)$ (Figure 5).

Special attention was paid to the interplay between the size of the configuration space, and the magnitude of the residual interaction within the pp -channel. It was found that as the first becomes larger, the second has to increase to obtain the agreement with the experimental data for the exclusive observables.

The main purpose of our discussion of exclusive properties was to put in evidence the limitations of the RPA and the QRPA models. The basic problem in the implementation of the RPA is the lack of pairing correlations, i.e. the inability for opening the $1p_{3/2}$ shell, while deficiency of the standard QRPA is in the non-conservation of the number of particles, as evidenced by the wave functions (3.1), (3.2), and (3.3) presented in Sec. III. In this way we have definitively established that the SM and the PQRPA are proper theoretical frameworks to describe

the ground state properties of ^{12}B and ^{12}N .⁶

The inclusive cross-sections $^{12}\text{C}(\nu, e^-)^{12}\text{N}$ and $^{12}\text{C}(\bar{\nu}, e^+)^{12}\text{B}$ have been studied within the PQRPA in the same manner as the exclusive ones for E_{ν_e} up to 300 MeV. As there are no experimental available in this case the comparison is done with the previous calculations only⁷, and displayed in Figures 6, and 7. Here, unlike within Figures 2, 3, and 4, we also show the results obtained with the other RPA-like models [34, 43, 51, 102], which could be a suitable framework for describing global nuclear properties such as it is the inclusive cross-sections.

When the size of the configuration space is enlarged the calculated PQRPA cross-sections, at difference with the exclusive ones, steadily increase, and particularly for neutrino energies larger than 200 MeV, in spite of including the particle-particle interaction. At low energy they approach to the cross section of the first-forbidden sum-rule limit, but are significantly smaller at high energies both for neutrino and antineutrino.

The largest space that we can deal within the number projection procedure is the one that includes all the orbitals until the $N = 6$ HO shell. This is the reason why we have recurred to the RQRPA where it is possible to employ larger configuration spaces. It seems that when the number of shells is increased to $N = 30$, and the cut-off energy E_{2qp} is large enough, the cross sections very likely converge as shown in Figures 8, 9, 10, and 11.

The Figure 10 also indicates that the RQRPA is a promising nuclear model to reproduce the quasi elastic $(\nu_\mu, ^{12}\text{C})$ cross section in the region of $E_{\nu_\mu} \sim 1$ GeV which has been measured recently at MiniBooNE [13]. We do not know whether the discrepancy between the experiment and the theory comes from the non completeness of the configuration space or from the smallness of the effective axial-vector coupling constant that we are using $g_A = 1$. It could also happens that we need $g_A = 1$ for the low energy exclusive cross section and $g_A = 1.255$ for the high energy inclusive cross section. We do not understand the reason for such a energy dependence of g_A , but it is consistent with the Eq. (23) in Ref. [114] where it is shown that for the low energy β -decay g_A could be much more quenched than the total GT strength. We hope to be able to say more on this matter in the next future.

We have also addressed the issue of multipole composition of the inclusive cross sections, by separating them into allowed ($J^\pi = 0^+, 1^+$), first-forbidden ($J^\pi = 0^-, 1^-, 2^-$), second-forbidden ($J^\pi = 2^+, 3^+$), and third-

⁶ After our work has been finished, Cheoun *et al.* [115] have presented a new evaluation of the ECS in ^{12}C within the QRPA. They get good agreement with data for $\bar{\sigma}_e(^{12}\text{N})$, which is at variance with the previous QRPA calculation [43].

⁷ As already mentioned in the introduction the only available experimental data on ^{12}C ICS is the low neutrino energy ($E_{\nu_e} < 60$ MeV) folded one, which has already been discussed in our previous works [49–51].

forbidden ($J^\pi = 3^-, 4^-$) processes. The results for the antineutrino reaction $^{12}\text{C}(\bar{\nu}, e^+)^{12}\text{B}$ are displayed in Figure 12 both for the PQRPA and the RQRPA. Of course, similar results are obtained also for neutrinos. We remark that the spectral functions $d\sigma_{e^+}^A(E_{\bar{\nu}})/dE_{\bar{\nu}}$, when evaluated within the PQRPA, clearly put into evidence the resonant structure of the allowed cross-section, which is mainly of the GT type.

The study of the partial ICSs has been related with the proposal done in Refs. [108, 109] of performing nuclear structure studies of forbidden processes by using low energy neutrino and antineutrino beams. From the results shown in Table I for the flux-averaged cross sections $\bar{\sigma}_{e^+}$ in the reaction $^{12}\text{C}(\bar{\nu}, e^+)^{12}\text{B}$ we show that the contribution of allowed transitions decreases gradually in favor of the first forbidden transitions according with the increase of γ -boost. We conclude that to study high forbidden reactions one would need $\bar{\nu}$ -fluxes with $E_{\bar{\nu}}$ up to $\gtrsim 150$ MeV in ^{12}C .

At the end we considered possible astrophysical applications of the $\nu/\bar{\nu}$ - ^{12}C nucleus folded cross sections $\bar{\sigma}_{e^\pm}$, using supernovae $\nu/\bar{\nu}$ spectra represented by a normalized Fermi-Dirac distribution with mean energy $\langle E_\nu \rangle \approx 3.15 \times T_\nu$, and zero chemical potential. It is found that for temperature $T_\nu = 3 - 5$ MeV both the PQRPA and RQRPA models yield significantly larger cross sections than the previously used shell model.

Acknowledgements

This work was partially supported by the Argentinean agency CONICET under contract PIP 0377, and by the U.S. DOE grants DE-FG02-08ER41533, DE-FC02-07ER41457 (UNEDF, SciDAC-2) and the Research Corporation. A.R.S. thanks to W.C. Haxton and G.M. Fuller for stimulating discussion and to the Institute of Nuclear Theory of University of Washington, where part of this work was performed. N. P. acknowledges support by the Unity through Knowledge Fund (UKF Grant No. 17/08), MZOS - project 1191005-1010 and Croatian National Foundation for Science.

Appendix A: Contributions to $\mathcal{T}_{J^\pi}(\kappa)$ of natural and unnatural parity states

The real and imaginary parts of the operators $\mathcal{O}_{\alpha J}$ given by (2.12) and (2.20) do not contribute simultaneously. In fact, the $\Re\mathcal{O}_{\alpha J}$ ($\Im\mathcal{O}_{\alpha J}$) contributes to natural (unnatural) parity states, which means that we always can work only with real operators, which greatly simplifies the calculations. To see this we note that, while the operators \mathcal{M}_J^V , \mathcal{M}_J^A , and

$$\mathcal{M}_{0J}^A = \sum_{L=J\pm 1} (-)^{(J-L-1)/2} F_{LJ0} j_L(\rho) [Y_L(\hat{\mathbf{r}}) \otimes \boldsymbol{\sigma}]_J, \quad (\text{A1})$$

are real, $\mathcal{M}_{\pm 1J}^A$ and $\mathcal{M}_{\pm 1J}^V$ are not. Explicitly,

$$\begin{aligned} \mathcal{M}_{\pm 1J}^A &= \mathcal{M}_{\pm 1J}^{A,R} + i\mathcal{M}_{\pm 1J}^{A,I} \\ \mathcal{M}_{\pm 1J}^V &= \mathcal{M}_{\pm 1J}^{V,R} + i\mathcal{M}_{\pm 1J}^{V,I} \end{aligned} \quad (\text{A2})$$

where

$$\begin{aligned} \mathcal{M}_{1J}^{A,R} &\equiv \mathcal{M}_{-1J}^{A,R} \\ &= \sum_{L=J\pm 1} (-)^{(J-L-1)/2} F_{LJ1} j_L(\rho) [Y_L(\hat{\mathbf{r}}) \otimes \boldsymbol{\sigma}]_J, \\ \mathcal{M}_{1J}^{A,I} &\equiv -\mathcal{M}_{-1J}^{A,I} = -F_{1J1} j_1(\rho) [Y_1(\hat{\mathbf{r}}) \otimes \boldsymbol{\sigma}]_J, \\ \mathcal{M}_{1J}^{V,R} &\equiv \mathcal{M}_{-1J}^{V,R} \\ &= \sum_{L=J\pm 1} (-)^{(J-L-1)/2} F_{LJ1} j_L(\rho) [Y_L(\hat{\mathbf{r}}) \otimes \boldsymbol{\nabla}]_J, \\ \mathcal{M}_{1J}^{V,I} &\equiv -\mathcal{M}_{-1J}^{V,I} = -F_{1J1} j_1(\rho) [Y_1(\hat{\mathbf{r}}) \otimes \boldsymbol{\nabla}]_J, \end{aligned} \quad (\text{A3})$$

with $L \geq 0$, and $J \neq 0$. Thus

$$\begin{aligned} \mathcal{O}_{\pm 1J} &= i(-g_A \pm \bar{g}_w)(\mathcal{M}_{1J}^{A,R} \pm i\mathcal{M}_{1J}^{A,I}) \\ &\quad + g_V(\mathcal{M}_{1J}^{V,R} \pm i\mathcal{M}_{1J}^{V,I}), \end{aligned} \quad (\text{A4})$$

and writing

$$\begin{aligned} \mathcal{O}_{0J} &= \mathcal{O}_{0J}^R + i\mathcal{O}_{0J}^I, \\ \mathcal{O}_{mJ} &= \mathcal{O}_{mJ}^R + i\mathcal{O}_{mJ}^I, \end{aligned} \quad (\text{A5})$$

it is not difficult to discover that:

- For natural parity states, with $\pi = (-)^J$, i.e., $J^\pi = 0^+, 1^-, 2^+, 3^-, \dots$:

$$\begin{aligned} \mathcal{O}_{0J}^R &= g_V \mathcal{M}_J^V, \\ \mathcal{O}_{0J}^I &= \frac{\tilde{k}_0}{\kappa} g_V \mathcal{M}_J^V, \\ \mathcal{O}_{\pm 1J}^R &= (\pm g_A - \bar{g}_w) \mathcal{M}_{1J}^{A,I} + g_V \mathcal{M}_{1J}^{V,R}, \end{aligned} \quad (\text{A6})$$

- For unnatural parity states, with $\pi = (-)^{J+1}$, i.e., $J^\pi = 0^-, 1^+, 2^-, 3^+, \dots$:

$$\begin{aligned} \mathcal{O}_{0J}^I &= -g_A \mathcal{M}_J^A - (\bar{g}_A + \bar{g}_{P1}) \mathcal{M}_{0J}^A, \\ \mathcal{O}_{0J}^R &= (g_A - \bar{g}_{P2}) \mathcal{M}_{0J}^A, \\ \mathcal{O}_{\pm 1J}^I &= (g_A \mp \bar{g}_w) \mathcal{M}_{1J}^{A,R} \mp g_V \mathcal{M}_{1J}^{V,I}. \end{aligned} \quad (\text{A7})$$

These operators have to be used in (2.22), instead of those defined in (2.12), and (2.20).

The correspondence between the individual matrix elements, defined by Donnelly, and Peccei in Eq (3.31) of Ref. [77], and the ones used here, is:

$$\begin{aligned} M_J &\rightarrow \mathcal{M}_J^V, \\ \Delta_J &\rightarrow \sqrt{2} \mathcal{M}_{1J}^{V,I}, \\ \Delta'_J &\rightarrow -\sqrt{2} \mathcal{M}_{1J}^{V,R}, \\ \Sigma_J &\rightarrow \sqrt{2} \mathcal{M}_{1J}^{A,I}, \\ \Sigma'_J &\rightarrow -\sqrt{2} \mathcal{M}_{1J}^{A,R}, \\ \Sigma_J'' &\rightarrow \mathcal{M}_{0J}^A, \\ \Omega_J &\rightarrow \mathcal{M}_J^A. \end{aligned} \quad (\text{A8})$$

Moreover, the correspondence between the linear combinations of these matrix elements defined in [77, Eqs. (3.32)] (for \hat{L}_J see [79, Eq. (14)]), and the ones introduced here is:

- For natural parity states :

$$\begin{aligned}\hat{M}_J &= O_{\emptyset J}, \\ \hat{L}_J &= O_{0J}, \\ \hat{T}_J^{\text{el}} \pm \hat{T}_J^{\text{mag}5} &= -\sqrt{2}O_{\pm 1J},\end{aligned}\quad (\text{A9})$$

- For unnatural parity states:

$$\begin{aligned}\hat{M}_J^5 &= O_{\emptyset J}, \\ -i\hat{L}_J^5 &= O_{0J}, \\ i(\hat{T}_J^{\text{el}5} \pm \hat{T}_J^{\text{mag}5}) &= \sqrt{2}O_{\pm 1J}.\end{aligned}\quad (\text{A10})$$

The following relation can also be useful:

$$\begin{aligned}O_{\emptyset J} &= \hat{\mathcal{M}}_J, \\ O_{mJ} &= \begin{cases} \hat{L}_J, & \text{for } m=0 \\ -\frac{1}{\sqrt{2}} [m\hat{T}_J^{\text{mag}} + \hat{T}_J^{\text{el}}], & \text{for } m=\pm 1 \end{cases},\end{aligned}\quad (\text{A11})$$

where $\hat{\mathcal{M}}_J = \hat{M}_J + \hat{M}_J^5$, $\hat{L}_J = \hat{L}_J + \hat{L}_J^5$, $\hat{T}_J^{\text{el}} = \hat{T}_J^{\text{el}} + \hat{T}_J^{\text{el}5}$, and $\hat{T}_J^{\text{mag}} = \hat{T}_J^{\text{mag}} + \hat{T}_J^{\text{mag}5}$.

The matrix elements of Kuramoto *et al.* [74] are related with our non-relativistic operators (2.14) as:

$$\begin{aligned}|\langle f|\hat{1}|i\rangle|^2 &= 4\pi \sum_{J_n^\pi} |\langle J_n^\pi || \mathcal{M}_J^V || 0^+ \rangle|^2, \\ |\langle f|\hat{\sigma}|i\rangle|^2 &= 4\pi \sum_{J_n^\pi} \sum_{m=0,\pm 1} |\langle J_n^\pi || \mathcal{M}_{mJ}^A || 0^+ \rangle|^2, \\ \Lambda &= \frac{4\pi}{3} \sum_{J_n^\pi} [|\langle J_n^\pi || \mathcal{M}_{0J}^A || 0^+ \rangle|^2 \\ &\quad - |\langle J_n^\pi || \mathcal{M}_{1J}^A || 0^+ \rangle|^2].\end{aligned}\quad (\text{A12})$$

In Ref. [74] are neglected the relativistic operators \mathcal{M}_J^A , and \mathcal{M}_{mJ}^V defined in (2.15).

Appendix B: Sum Rule Approach

We follow here the sum-rule approach developed by Kuramoto *et al.* [74], and adapt it to our formalism. We start from Eqs. (2.25), and (2.27), and as in this work we assume that the $\omega_{J_n^\pi}$ dependence of the integrand can be ignored, fixing it at a representative value $\overline{\omega_{J_n^\pi}}$. The summation over final nuclear states J_n^π then can be carried out by closure, and the ICS is

$$\begin{aligned}\sigma_\ell^{SR}(E_\nu) &= G^2 \frac{|\mathbf{p}_\ell| E_\ell}{2\pi} F(Z+S, E_\ell) \\ &\quad \times \int_{-1}^1 d(\cos\theta) \mathcal{T}^{SR},\end{aligned}\quad (\text{B1})$$

where the lepton energy is $E_\ell = E_\nu - \overline{\omega_{J_n^\pi}}$, while the sum-rule matrix element reads:

$$\begin{aligned}\mathcal{T}^{SR} &= \sum_{\alpha=\emptyset,0,\pm 1} \langle 0^+ | O_\alpha^\dagger O_\alpha | 0^+ \rangle \mathcal{L}_\alpha \\ &\quad - 2\Re \left(\langle 0^+ | O_\emptyset^\dagger O_0 | 0^+ \rangle \mathcal{L}_{\emptyset 0} \right).\end{aligned}\quad (\text{B2})$$

The operators O_α are given by (2.6), and the lepton traces by [49, Eq. (2.24)]. The matrix elements in (B2) are proportional to $N(1-D)$, where N_N is the number of neutrons (protons), contained in the target nucleus for the neutrino (anti-neutrino) reaction. The correlation functions D come from the Pauli-exclusion-effect, and depend on the type of the operator. One gets:

$$\mathcal{T}^{SR} = N_N \left(T_\emptyset \mathcal{L}_\emptyset + \sum_M T_M \mathcal{L}_M - 2T_{\emptyset 0} \mathcal{L}_{\emptyset 0} \right), \quad (\text{B3})$$

with

$$\begin{aligned}T_\emptyset &\equiv g_V^2(1-D_S) + (\overline{g}_A + \overline{g}_{P1})^2(1-D_L), \\ T_0 &\equiv \overline{g}_V^2(1-D_S) + (g_A - \overline{g}_{P2})^2(1-D_L), \\ T_1 &\equiv (g_A - \overline{g}_W)^2(1-D_T), \\ T_{-1} &\equiv (g_A + \overline{g}_W)^2(1-D_T), \\ T_{\emptyset 0} &\equiv -g_V \overline{g}_V (1-D_S) + (\overline{g}_A + \overline{g}_{P1})(g_A - \overline{g}_{P2})(1-D_L).\end{aligned}\quad (\text{B4})$$

The correlation functions D_S, D_L and D_T were taken from the SM calculation done by Bell, and Llewellyn Smith [116] with HO wave functions, and representing the nuclear ground state by a single determinant wave function. The results for ^{12}C are [116, Table 1]):

$$\begin{aligned}D_S &= e^{-\eta} [1 + 0.148\eta^2], \\ D_T &= e^{-\eta} [0.704 + 0.148\eta + 0.148\eta^2], \\ D_L &= e^{-\eta} [0.704 + 0.296\eta + 0.148\eta^2],\end{aligned}\quad (\text{B5})$$

where $\eta = \frac{1}{2}b^2\kappa^2 \cong 0.0558$.

As seen from (2.26), the factor $|\mathbf{p}_\ell| E_\ell$ in (B1) behaves as $(E_\nu - \overline{\omega_{J_n^\pi}})^2$, and therefore $\sigma_\ell^{SR}(E_\nu)$ depends very critically on the average value for the excitation energy $\overline{\omega_{J_n^\pi}}$.

$$\begin{aligned}E_\ell &= E_\nu - \omega_{J_n^\pi}, \quad |\mathbf{p}_\ell| = \sqrt{(E_\nu - \omega_{J_n^\pi})^2 - m_\ell^2}, \\ \kappa &= |\mathbf{p}_\ell - \mathbf{q}_\nu| \\ &= \sqrt{2E_\nu(E_\ell - |\mathbf{p}_\ell| \cos\theta) - m_\ell^2 + \omega_{J_n^\pi}^2},\end{aligned}\quad (\text{B6})$$

Appendix C: Extreme Relativistic Limit

Using the present formalism the ERL, defined by the limit of the lepton velocity $|\mathbf{p}_\ell|/E_\ell \rightarrow 1$, yields

$$\sigma_\ell^{ERL}(E_\nu) = \sum_{J_n^\pi} \frac{E_\ell^2}{2\pi} F(Z+S, E_\ell) \int_{-1}^1 d(\cos\theta) \mathcal{T}_{J_n^\pi}^{ERL}(\kappa), \quad (\text{C1})$$

with

$$\kappa = \sqrt{2E_\nu E_\ell(1 - \cos\theta) + \omega_{J_n^\pi}^2}, \quad (\text{C2})$$

and

$$\begin{aligned} \mathcal{T}_{J_n^\pi}^{ERL}(\kappa) &= 4\pi G^2 \left[2 \cos^2 \frac{\theta}{2} \left| \langle J_n^\pi || \mathcal{O}_{0J}(\kappa) - \frac{k_\theta}{\kappa} \mathcal{O}_{0J}(\kappa) || 0^+ \rangle \right|^2 \right. \\ &+ \sum_{m=\pm 1} |\langle J_n^\pi || \mathcal{O}_{mJ}(\kappa) || 0^+ \rangle|^2 \\ &\times \left(\frac{k^2}{\kappa^2} \cos^2 \frac{\theta}{2} + 2 \sin^2 \frac{\theta}{2} \right. \\ &\left. \left. + 2mS \sin \frac{\theta}{2} \sqrt{\frac{k^2}{\kappa^2} \cos^2 \frac{\theta}{2} + \sin^2 \frac{\theta}{2}} \right) \right]. \quad (\text{C3}) \end{aligned}$$

Appendix D: Muon Capture rate

For the sake of completeness we also show the formula for the muon capture process within the present formalism. Here $\kappa = E_\nu = m_\mu - \omega_{J_n^\pi} - \Delta M - E_B$, where E_B^μ is the binding energy of the muon in the $1S$ orbit, and instead of (2.5) one has:

$$\begin{aligned} \bar{g}_V &= g_V \frac{E_\nu}{2M}; \quad \bar{g}_A = g_A \frac{E_\nu}{2M}, \\ \bar{g}_W &= (g_V + g_M) \frac{E_\nu}{2M}; \quad \bar{g}_P = g_P \frac{E_\nu}{2M}, \quad (\text{D1}) \end{aligned}$$

where $\bar{g}_P = \bar{g}_{P2} - \bar{g}_{P1}$. The muon capture transition rate reads

$$\Lambda(\omega_{J_n^\pi}) = \frac{E_\nu^2}{2\pi} |\phi_{1S}|^2 \mathcal{T}_\Lambda(\omega_{J_n^\pi}), \quad (\text{D2})$$

where ϕ_{1S} is the muonic bound state wave function evaluated at the origin, and

$$\begin{aligned} \mathcal{T}_\Lambda(\omega_{J_n^\pi}) &= 4\pi G^2 \left[|\langle J_n^\pi || \mathcal{O}_{0J}(E_\nu) - \mathcal{O}_{0J}(E_\nu) || 0^+ \rangle|^2 \right. \\ &\left. + 2 |\langle J_n^\pi || \mathcal{O}_{-1J}(E_\nu) || 0^+ \rangle|^2 \right], \quad (\text{D3}) \end{aligned}$$

with

- For natural parity states, with $\pi = (-)^J$, i.e., $J^\pi = 0^+, 1^-, 2^+, 3^-, \dots$:

$$\begin{aligned} \mathcal{O}_{0J} - \mathcal{O}_{0,J} &= g_V \frac{m_\mu - \Delta E_{\text{Coul}} - E_B}{E_\nu} \mathcal{M}_J^V, \\ \mathcal{O}_{-1J} &= -(g_A + \bar{g}_W) \mathcal{M}_{-1J}^{A,I} + g_V \mathcal{M}_{-1J}^{V,R}, \quad (\text{D4}) \end{aligned}$$

and

- For unnatural parity states, with $\pi = (-)^{J+1}$, i.e., $J^\pi = 0^-, 1^+, 2^-, 3^+, \dots$:

$$\begin{aligned} \mathcal{O}_{0J} - \mathcal{O}_{0,J} &= g_A \mathcal{M}_J^A + (g_A + \bar{g}_A - \bar{g}_P) \mathcal{M}_{0J}^A, \\ \mathcal{O}_{-1J} &= -(g_A + \bar{g}_W) \mathcal{M}_{-1J}^{A,R} - g_V \mathcal{M}_{-1J}^{V,I}. \quad (\text{D5}) \end{aligned}$$

-
- [1] C. Athanassopoulos *et al.* [LSND Collaboration], Phys. Rev. C **54**, 2685 (1996); *ibid* Phys. Rev. Lett. **77**, 3082 (1996).
- [2] C. Athanassopoulos *et al.* [LSND Collaboration], Phys. Rev. C **58**, 2489 (1998); *ibid* Phys. Rev. Lett. **81**, 1774 (1998).
- [3] A. Aguilar *et al.* [LSND collaboration], Phys. Rev. D **64**, 112007 (2001).
- [4] Y. Fukuda *et al.* [Super-Kamiokande Collaboration], Phys. Rev. Lett. **81**, 1562 (1998); Y. Ashie *et al.* [Super-Kamiokande Collaboration], Phys. Rev. Lett. **93**, 101801 (2004).
- [5] B. Aharmim *et al.* [SNO Collaboration], Phys. Rev. C **59**, 055502 (2005); M. B. Smy *et al.* [Super-Kamiokande Collaboration], Phys. Rev. D **69**, 011104 (2004).
- [6] T. Araki *et al.* [KamLAND Collaboration], Phys. Rev. Lett. **94**, 081801 (2005).
- [7] M. H. Ahn *et al.* [K2K Collaboration], Phys. Rev. Lett. **90**, 041801 (2003).
- [8] R. Maschuw *et al.* [KARMEN Collaboration], Prog. Part. Phys. **40**, (1998) 183; and references therein mentioned.
- [9] B. Armbruster *et al.* [KARMEN collaboration], Phys. Rev. D **65**, 112001 (2002).
- [10] R. C. Allen *et al.*, Phys. Rev. Lett. **64**, 1871 (1990).
- [11] D. A. Krakauer *et al.*, Phys. Rev. C **45**, 2450 (1992).
- [12] A. A. Aguilar-Arevalo *et al.* (SciBooNE Collaboration), arXiv:hep-ex/0601022.
- [13] A. A. Aguilar-Arevalo *et al.* (MiniBooNE Collaboration), Nucl. Instrum. Methods A **599**, 28 (2009).
- [14] Y. Efremenko, Nucl. Phys. **B138**(Proc. Suppl.), 343 (2005); F.T. Avignone III and Y.V. Efremenko, J. Phys. G **29**, 2615 (2003).
- [15] N.Yu. Agafonova *et al.*, Astron. Phys. **27**, 254 (2007).
- [16] M. Fukugita, Y. Kohyama and K. Kubodera, Phys. Lett. **B212**, 139 (1988).
- [17] D. Autiero *et al.*, J. Cosmol. Astropart. Phys. **0711**, 011 (2007); arXiv:hep-ph/0705.0116.
- [18] C. Lunardini and A. Y. Smirnov, J. Cosmol. Astropart. Phys. **0306**, 009 (2003).
- [19] A. S. Dighe, M. T. Keil, and G. G. Raffelt, J. Cosmol. Astropart. Phys. **0306**, 005 (2003).
- [20] H. Duan, G. M. Fuller, J. Carlson, and Y.-Q. Zhong, Phys. Rev. Lett. **99**, 241802 (2007).
- [21] B. Dasgupta, A. Dighe, and A. Mirizzi, Phys. Rev. Lett. **101**, 171801 (2008).
- [22] B. Dasgupta, A. Mirizzi, I. Tamborra, and R. Tomas, Phys. Rev. **D81**, 093008 (2010).
- [23] M. Mezzetto and T. Schwetz, arXiv:1003.5800v1 [hep-ph] (2010).
- [24] A. Strumia and F. Vissani, arXiv: hep-ph/0606054v2.
- [25] C. Athanassopoulos *et al.* [LSND Collaboration], Phys. Rev. C **55**, 2078 (1997).
- [26] L. B. Auerbach *et al.* [LSND Collaboration], Phys. Rev.

- C **64**, 065501 (2001).
- [27] B. Zeitnitz *et al.*[KARMEN Collaboration], Prog. Part. Nucl. Phys. **40**, 169 (1998).
- [28] C. Athanassopoulos *et al.* [LSND Collaboration], Phys. Rev. C **56**, 2806 (1997).
- [29] L. B. Auerbach *et al.*[LSND Collaboration], Phys. Rev. C **66**, 015501 (2002).
- [30] LSND home page, <http://www.nu.to.infn.it/exp/all/lsnd/>
- [31] Tepei Katori, in The 5th International Workshop on Neutrino-Nucleus Interactions in the Few-GeV Region, edited by GERALYN P. ZELLER, JORGE G. MORFIN, FLAVIO CAVANNA, AIP Conf. Proc. No. 967 (AIP, New York, 2007), p. 123; A.A. Aguilar-Arevalo *et al.*, Phys. Rev. Lett. **103**, 081801 (2009); Phys. Rev. D **81**, 013005 (2010).
- [32] A. Rodriguez, *et al.*, Phys. Rev. D **78**, 032003 (2008).
- [33] Y. Kurimoto *et al.*, Phys. Rev. D **81**, 033004 (2010).
- [34] J.S. O'Connell, T.W. Donnelly and J.D. Walecka, Phys. Rev. C **6**, 719 (1972).
- [35] T.W. Donnelly, Phys. Rev. C **1**, 853 (1970).
- [36] B.A. Brown and B.H. Wildenthal, At. Data Nucl. Data Tables **33**, 347 (1985).
- [37] H. Castillo and F. Krmpotić, Nucl. Phys. **A469**, 637 (1987).
- [38] F. Osterfeld, Rev. Mod. Phys. **64**, 491 (1992), and references therein.
- [39] G. Martínez-Pinedo *et al.*, Phys. Rev. C **53**, R2602 (1996).
- [40] E. Kolbe, K. Langanke and S. Krewald, Phys. Rev. C **49**, 1122 (1994).
- [41] E. Kolbe, K. Langanke and P.Vogel, Phys. Rev. C **50**, 2576 (1994).
- [42] A.C. Hayes and I.S. Towner, Phys. Rev. C **61**, 044603 (2000).
- [43] C. Volpe, N. Auerbach, G. Colò, T. Suzuki, N. Van Giai, Phys. Rev. C **62**, 015501 (2000).
- [44] T. Suzuki *et al.*, Phys. Rev. C **74**, 034307 (2006).
- [45] G. H. Miller *et al.*, Phys. Lett. **B41**, 50 (1972).
- [46] D.F. Measday, Phys. Rep. **354**, 243 (2001).
- [47] T.J. Stocki *et al.*, Nucl. Phys. **A697**, 55 (2002).
- [48] F. Krmpotić, A. Mariano and A. Samana, Phys. Lett. **B541**, 298 (2002).
- [49] F. Krmpotić, A. Samana, and A. Mariano, Phys. Rev. C **71**, 044319 (2005).
- [50] A. Samana, F. Krmpotić, A. Mariano and R. Zukanovich Funchal, Phys. Lett. **B642**, 100 (2006).
- [51] N. Paar, D. Vretenar, T. Marketin and P. Ring, Phys. Rev. C **77**, 024608 (2008).
- [52] T. Marketin, N. Paar, T. Nikšić and D. Vretenar, Phys. Rev. C **79**, 054323 (2009).
- [53] K. Hagino and H. Sagawa, Nucl. Phys. **A695**, 82 (2001).
- [54] V. Rodin and A. Faessler, Phys. Rev. C **77**, 025502 (2008).
- [55] R.A. Smith and E.J. Moniz, Nucl. Phys. **B43**, 605 (1972).
- [56] J. Nieves, J.E. Amaro, and M. Valverde, Phys. Rev. C **70**, 055503 (2004).
- [57] M. Valverde, J.E. Amaro, and J. Nieves, Phys. Lett. **B638**, 325 (2006). Phys. Rev. C **77**, 025502 (2008).
- [58] C. Mahaux, P.E. Bortignon, R.A. Broglia, and C.H. Dasso, Phys. Rep. **120**, 1 (1985).
- [59] G. Jacob and T. A. J. Maris, Rev. Mod. Phys. **45**, 6 (1973).
- [60] S. Frullani and J. Mougey, Adv. Nucl. Phys. **14**, 1 (1984).
- [61] S.L. Belostotskii *et al.*, Sov. J. Nucl. Phys. **41**, 903 (1985); S.S. Volkov *et al.*, Sov. J. Nucl. Phys. **49**, 848 (1990).
- [62] M. Leuschner *et al.*, Phys. Rev. C **49**, 955 (1994).
- [63] T. Yamada, M. Takahashi, and K. Ikeda, Phys. Rev. C **53**, 752 (1996).
- [64] T. Yamada, Nucl. Phys. **A687**, 297c (2001).
- [65] M. Yosoi *et al.*, Phys. Lett. **B551**, 255 (2003).
- [66] T. Yamada, M. Yosoi, and H. Toyokawa, Nucl. Phys. **A738**, 323 (2004).
- [67] K. Kobayashi *et al.*, arXiv:nucl-ex/0604006.
- [68] J. E. Amaro, M. B. Barbaro, J. A. Caballero, T. W. Donnelly, and C. Maieron, Phys. Rev. C **71**, 065501 (2005).
- [69] E. Kolbe, K. Langanke, G. Martínez-Pinedo and P. Vogel, J. Phys. **G29**, 2569 (2003).
- [70] K. S. Kim, Myung-Ki Cheoun, and Byung Geel Yu, Phys. Rev. C **77**, 054604 (2008).
- [71] A. V. Butkevich, Phys. Rev. C **78**, 015501 (2008); Phys. Rev. C **80**, 014610 (2009); arXiv:1006.1595.
- [72] T. Leitner, O. Buss, L. Alvarez-Ruso, and U. Mosel Phys. Rev. C **79**, 034601 (2009).
- [73] M. Martini, M. Ericson, G. Chanfray and J. Marteau, Phys. Rev. C **80**, 065501 (2009).
- [74] T. Kuramoto *et al.*, Nucl. Phys. **A512**, 711 (1990).
- [75] P. Vogel and M.R. Zirnbauer, Phys. Rev. Lett. **57**, 3148 (1986).
- [76] D. Cha, Phys. Rev. **C27**, 2269 (1983).
- [77] T. W. Donnelly and R. D. Peccei, Phys. Rep. **50**, 1 (1979).
- [78] J.D. Walecka, *Theoretical Nuclear and Subnuclear Physics, Oxford University Press, New York*, 531 (1995).
- [79] T.W. Donnelly and W.C. Haxton, Atomic Data and Nuclear Data Tables **23**, 103 (1979).
- [80] F. Krmpotić, K. Ebert, and W. Wild, Nucl. Phys. **A342**, 497 (1980); F. Krmpotić, Phys. Rev. Lett. **46**, 1261 (1981).
- [81] H. Behrens and W. Bühring, *Electron Radial Wave Functions and Nuclear Beta Decay* (Clarendon, Oxford, 1982), and references therein.
- [82] R.J. Blin-Stoyle and S.C.K. Nair, Advances in Physics **15**, 493 (1966).
- [83] J. Engel, Phys. Rev. C **57**, 2004 (1998).
- [84] A.R. Samana and C.A. Bertulani, Phys. Rev. C **78**, 024312 (2008)
- [85] J. Hirsch and F. Krmpotić, Phys. Rev. C **41**, 792 (1990), *ibid* Phys. Lett. **B246**, 5 (1990).
- [86] F. Krmpotić, J. Hirsch and H. Dias, Nucl. Phys. **A542**, 85 (1992).
- [87] F. Krmpotić, A. Mariano, T.T.S. Kuo, and K. Nakayama, Phys. Lett. **B319**, 393 (1993).
- [88] F. Krmpotić and Shelly Sharma, Nucl. Phys. **A572**, 329 (1994).
- [89] A.R. Samana, F. Krmpotić and C.A. Bertulani, Comp. Phys. Comm. **181**, 1123 (2010).
- [90] N. Paar, T. Nikšić, D. Vretenar, and P. Ring, Phys. Rev. C **69**, 054303 (2004).
- [91] G. A. Lalazissis, T. Nikšić, D. Vretenar, and P. Ring, Phys. Rev. C **71**, 024312 (2005).
- [92] J. F. Berger, M. Girod, and D. Gogny, Comp. Phys. Comm. **63**, 365 (1991).
- [93] N. Paar, P. Ring, T. Nikšić, and D. Vretenar, Phys. Rev. C **67**, 034312 (2003).
- [94] N. Paar, D. Vretenar, E. Khan, and G. Colò, Rep. Prog.

- Phys. **70**, 691 (2007).
- [95] F. Ajzenberg-Selove, Nucl. Phys. **A 433**, 1(1985); TUNL Nuclear Data Evaluation Project. Webpage: <http://www.tunl.duke.edu/nucldata/>.
- [96] D. E. Alburger and A.M. Nathan, Phys. Rev. C **17**, 280 (1978).
- [97] A. Strumia and F. Vissani, arXiv.org/abs/hep-ph/0606054
- [98] J. Engel, E. Kolbe, K. Langanke, and P. Vogel, Phys. Rev. C **54**, 2740 (1996).
- [99] E. Kolbe, K. Langanke and G. Martínez-Pinedo, Phys. Rev. C **60**, 052801(R) (1999).
- [100] F. Krmpotić, K. Nakayama, and A. P. Galeão, Nucl. Phys. **A339**, 475 (1983).
- [101] H. Budd, A. Bodek, and J. Arrington, [arXiv:hep-ex/0308005](http://arXiv.org/abs/hep-ex/0308005).
- [102] E. Kolbe, K. Langanke and P. Vogel Nucl. Phys. **A652**, 91 (1999).
- [103] M. Martini, M. Ericson, G. Chanfray and J. Marteau, Phys. Rev. C **81**, 045502 (2010).
- [104] E. Bauer, and G. Garbarino, Phys. Rev. C **81**, 064315 (2010).
- [105] A. Mariano, E. Bauer, F. Krmpotić, and A.F.R. de Toledo Piza, Phys. Lett. **B268**, 332 (1991).
- [106] D. Van Neck, M. Waroquier, V. Van der Sluys, and J. Ryckebusch, Phys. Lett. **B274**, 142(1992).
- [107] A. Mariano, F. Krmpotić, and A.F.R. de Toledo Piza, Phys. Rev. C **49**, 2824 (1994), and Phys. Rev. C **53**, 1664 (1996).
- [108] R. Lazauskas and C. Volpe, Nucl. Phys. **A792**, 219 (2007).
- [109] C. Volpe, J. Phys. G **30**, L1 (2004); [arXiv:hep-ph/0303222](http://arXiv.org/abs/hep-ph/0303222).
- [110] S. E. Woosley, D. H. Hartmann, R. D. Hoffman and W. C. Haxton, Ap. J. **356**, 272 (1990).
- [111] M. Th. Keil, G. G. Raffelt, and H. -Th. Janka, Ap. J. **590**, 971 (2003).
- [112] E.Kh. Akhmedov, Lectures given at Trieste Summer School in Particle Physics, June 7-9, 1999; [arXiv:hep-ph/0001264v2](http://arXiv.org/abs/hep-ph/0001264v2).
- [113] H. Duan, G. M. Fuller, J. Carlson, and Y-Z. Qian, Phys. Rev. Lett. **99**, 241802 (2007); H. Duan, G. M. Fuller and Y.Z. Qian, J. Phys. G **36**, 113201 (2009).
- [114] K. Nakayama, A. P. Galeão, and F. Krmpotić, Phys. Lett. **B114**, 217 (1982).
- [115] M. K Cheoun *et al.*, Phys. Rev. C **81**, 028501 (2010).
- [116] J.S. Bell and C.H. Llewellyn Smith, Nucl. Phys. **B28**, 317 (1971).